Titre: Title:	On the exploration of the melting behavior of metallic compounds and solid solutions via multiple classical molecular dynamics approaches: application to Al-based systems
Auteurs: Authors:	Camille Rincent, Juan-Ricardo Castillo-Sánchez, Aïmen E. Gheribi, & Jean-Philippe Harvey
Date:	2023
Type:	Article de revue / Article
Référence: Citation:	Rincent, C., Castillo-Sánchez, J.-R., Gheribi, A. E., & Harvey, J.-P. (2023). On the exploration of the melting behavior of metallic compounds and solid solutions via multiple classical molecular dynamics approaches: application to Al-based systems. Physical Chemistry Chemical Physics, 25(15), 10866-10884. https://doi.org/10.1039/d3cp00912b

URL de PolyPublie: PolyPublie URL:	https://publications.polymtl.ca/53578/
Version:	Version finale avant publication / Accepted version Révisé par les pairs / Refereed
Conditions d'utilisation: Terms of Use:	Tous droits réservés / All rights reserved

Document publié chez l'éditeur officiel
Document issued by the official publisher

Titre de la revue: Journal Title:	Physical Chemistry Chemical Physics (vol. 25, no. 15)
Maison d'édition: Publisher:	The Royal Society of Chemistry
URL officiel: Official URL:	https://doi.org/10.1039/d3cp00912b
Mention légale: Legal notice:	

On the exploration of the melting behavior of metallic compounds and solid solutions via multiple classical molecular dynamics approaches: application to Al-based systems

Camille Rincent, Ricardo Castillo, Aïmen E. Gheribi, Jean-Philippe Harvey

ᵃCRCT - Polytechnique Montreal, Box 6079, Station Downtown, Montreal, QC, Canada

Abstract

Classical molecular dynamics simulations of metallic systems have been extensively applied in recent years for the exploration of the energetic behavior of mesoscale structures and for the generation of thermodynamic and physical properties. The evaluation of the conditions leading to the melting of pure metals and alloys is particularly challenging as it involves at one point the simultaneous presence of both a solid and a liquid phase. Defects such as vacancies, dislocation, grain boundaries and pores typically promote the melting of a solid by locally increasing its free energy which favors the destruction of long-range ordering at the origin of this phase transition. In real materials, many of these defects are microscopic and cannot yet be modelled via conventional atomistic simulations. Still, molecular dynamics-based methodologies are commonly used to estimate the melting temperature of solids. These methods involve the use of mesoscale supercells with various nanoscale defects. Moreover, the deterministic nature of classical MD simulations requires the adequate selection of the initial configuration to be melted. e numerical experiments.

In this context, the main objective of this paper is to quantify the precision of the existing classical molecular dynamics computational methods used to evaluate the melting point of pure compounds as well as the solidus/liquidus lines of Al-based binary metallic systems. We also aim to improve the methodology of different approaches such as the void method, the interface method as well as the grain method to obtain a precise evaluation of the melting behavior of pure metals and alloys. We carefully analyzed the importance of the local chemical ordering on the melting behavior. The ins and outs of different numerical methods in predicting the melting temperature via MD are discussed through several examples related to pure metallic elements, congruently and non-congruently melting compounds as well as binary solid solutions. It is shown that the defect distribution of the initial supercell configuration plays an important role upon the description of the melting mechanism of solids leading to a poor predictive capability of melting temperature if not properly controlled. A new methodology based on defect distribution within the initial configuration is proposed to overcome these limitations.

Keywords: Large-scale Molecular Dynamics simulations, Melting dynamics, Phase transition, Liquidus, Solidus, 2NN-MEAM force field

1. Introduction

The field of alloy engineering has grown vastly in the last few years, delving into a deeper understanding of the thermo-physical behavior of specific metallic materials such as high entropy alloys [1, 2]. These new materials find applications at high temperature [3, 4, 5] such as in corrosive gaseous environments like combustion chambers [6]. The methodology consisting in integrating multi-scale models (based on both quantum and classical energetic description of condensed phases) to evaluate and predict the thermo-physical and mechanical properties of a material [7] is known as Integrated
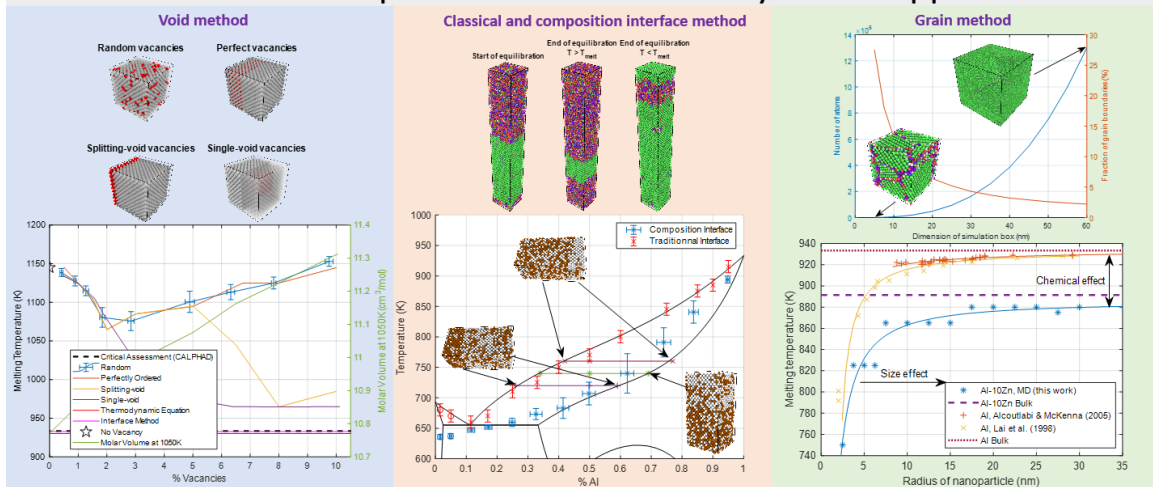
Figure 1: Graphical Abstract.

Computational Materials Engineering (ICME) [8, 9]. At the nano/atomic scale, this engineering principle is applied through atomistic simulations such as molecular dynamics (MD) and Monte Carlo (MC) methods [10, 11]. Atomistic simulations have demonstrated robustness for alloy design, e.g., tailoring nanomaterials' crystallography by controlling the cooling rate [12]. On one side, conventional MC simulations performed in the NPT, NVT and NVE ensembles cannot directly access dynamic properties as they rely on time-independent iterations (i.e. atom displacement and permutation as well as supercell volumetric changes) based on energy differences and Boltzmann distributions. On the other side, MD simulations are designed to access these dynamic properties but suffer from a poor exploration of the phase space caused by the short simulation times as well as the presence of energy barriers (especially in the solid state) [13]. Some hybrid MD-MC methods have been developed to circumvent these limitations and provide access to dynamic properties from a more complete phase space exploration [14]. In both types of atomistic simulations, either classical interatomic potentials or quantum-based *ab initio* calculations can be used to describe the energetics of the condensed systems at a given time/iteration.

Simulation tools are both effective and helpful to discover new alloys as it considerably lowers the investment cost of exploring the experimental properties of alloys. Experiments are time-consuming and require an initial investment in equipment [15] which often slows down and greatly limits material development. As such, simulations also help to compensate for the lack of experimental data, especially for multicomponent single-phase systems [16, 17]. Aluminum is a common alloying element to these alloys [18, 19]. Atomistic simulations to study its alloying effect on the thermo-physical properties of metallic materials have been mostly explored up to now for binary [20, 21, 22, 23] and ternary systems [24, 25, 26]. When exploring the current literature on higher-order and highly-alloyed systems (such as high entropy alloys), the amount of valuable data is scarce. One precise approach to alleviate the lack of data for metallic systems are quantum-based molecular dynamics simulations (also called *Ab-Initio* Molecular Dynamics or AIMD) typically carried in the framework of Density Functional Theory (DFT). The *Ab-Initio* nature of this approach provides an accurate prediction of the electronic structure and the resulting internal energy of metallic condensed phases but quickly becomes too computationally costly when applied to the energetic description of large-scale systems (i.e. thousands or more atoms) [27, 28]. They are also limited to very short simulated times (i.e. nano-second scale), leading to inaccurate estimations of dynamic properties (such as the viscosity, thermal conductivity,

and self-diffusivity) [29]. Moreover, effects of impurities or alloying elements in dilute amounts on the equilibrium properties are not accessible due to the small system size. Classical molecular dynamics are a more efficient atomistic simulation scheme for such conditions, as it can simulate large-scale systems, yielding results for a wide range of chemical composition of the simulated supercell (including dilute regions) at the expense of a less precise description of the chemical interactions in the system [30, 31, 32].

Collections of both experimental and numerical thermodynamic properties on such metallic systems are used to build CALPHAD (CALculation of PHAse Diagrams) databases. These are the core of modern computational thermochemistry, which is the only effective theory at the moment to accurately predict multi-phasic phase assemblage equilibria. DFT data are nowadays integrated in the CALPHAD modeling of solid phases [33]. Unfortunately, the systematic generation of sets of self-consistent thermodynamic data via DFT simulations to construct complete and accurate thermodynamic databases is still not achievable at this time. Novel simulation methods in classical molecular dynamics (MD) are being explored in order to attain a better understanding of ternary and high-order systems and to overcome these limitations. If one wants to generate accurate thermodynamic properties, classical MD requires a precise, self-consistent and complete database of interatomic potentials [34]. Their applicability and transferability to large scale multicomponent systems which are required to describe alloys [35, 36, 37] need to be verified/tested with both experimental data and DFT calculations. Despite this being a critical objective, we must first perfect the simulation methodology to combine a classical approach, reliable interatomic potentials and methodologies, while respecting constraints such as reasonable simulation times and a big enough system size to consider the impact of chemistry.

One popular approach to tune an interatomic potential is to approximate the force field experienced by the atoms of a given condensed phase structure calculated from DFT simulations using semi-empirical formalisms. In our work the modified embedded atom model within the second nearest-neighbor approximation (2NN-MEAM) formalism (which explicitly accounts for the effect of the embedding effect of the electronic cloud surrounding the atomic nuclei) is used [38]. This is an easy to parameterize interatomic potential with a limited number of fitting parameters. It has been well documented by Lee and Baskes who have repeatedly shown its robustness and applicability to metallic systems [38, 39, 34, 40, 41, 42].

Classical MD is a powerful tool that provides access to sets of self-consistent thermodynamic (enthalpy of formation of solids, enthalpy of mixing of liquids) and dynamic properties (such as viscosity, thermal conductivity) of unary and binary metallic systems [43, 44]. These classical MD studies typically use the melting behavior of the system (i.e. the melting temperature of pure metals or the liquidus/solidus temperature in the case of multicomponent solid phases) as a benchmark phase transition to validate the precision and transferability of the interatomic potentials [45, 37]. This first-order transition is directly connected to the strength of the chemical interactions in both the solid and the liquid [46]. For macroscopic solid phases, point (vacancies), line (dislocations), planar (grain boundaries) and volumetric (pores) defects which increase the total energy of the bulk material are numerous. Such defects make the melting process much easier and lower the melting point when compared to a perfect mono-crystal, since melting starts from grain boundaries [47, 48]. In such bulk materials, defect concentrations can be potentially quite high; as an example, the fraction of vacancies close to melting for pure tungsten is about 1.6% [49], and around 0.09% in pure aluminium [50]. At the meso-scale which is currently accessible with modern computational resources (i.e. millions of atoms in classical MD), the potential grain size and scale of the other metallurgical features which can be modelled is much smaller than for real materials. Therefore each defect introduced in the system has a more pronounced effect on the energetics of the solid structure. One important challenge is to adjust and tune the number and type of defects introduced in an originally perfect lattice to adequately modulate its energetic stability. Additionally, in the framework of material design, the accurate prediction of phase change behavior of new materials is a key characteristic to be able to accurately define, which can be studied in MD [51].

Currently in the literature these melting point evaluations are performed using a variety of direct techniques such as the void or defect method [52, 53, 54], the interface method [54] and the grain

method [55, 47, 48]. The defect method works by creating perfect lattices and introducing defects to mechanically destabilize the solid structure [56, 57, 58]. The interface method is based on the creation of a solid/liquid interface. This interface progresses toward either the solid or the liquid region depending on the imposed equilibrium conditions. This technique overcomes the overheating artefact observed for the melting of defect-free solid structures [59, 60]. As it will be presented in this work, the interface method which is more complex to implement yields roughly the same results as the void method when a careful distribution of defects into the supercell is performed, which has also been confirmed in the past through other projects [61]. This showcases not only the importance and value into rethinking the way classical molecular dynamics simulation should be built from their initial structure, but also the strength inherent to the void method thanks to its ability to consider the chemistry of simulated solid. A summary of multiple melting MD methods and their implementation details are presented in table 1. Overall, simulation practices are different from one reference to anotheer. Besides, the simulation details are typically overlooked, which compromises the reproductibility of reported data in the literature. Therefore, a comprehensive study of the simulation setup is required to standardize the MD's melting strategies.

This work evaluates three conventional MD methods (i.e. voids technique, interface procedure, and grain approach) to predict the melting temperature of elements, stoichiometric compounds, and disorder phases. The void method has been extended to multiple spatial distributions in order to assess the effect of the vacancies' chemical environment. Particular attention is given to the nature of each solid and its relationship with the mechanical stability before the melting process. For the congruently melting scenario, the Al_3Zr intermetallic is explored in its stable form ($D0_{23}$) and with two metastable configurations ($L1_2$ and disordered FCC phase). For the case of a peritectic intermetallic's melting, the ω-Al_4Cr [71] compound is examined. The importance of the site distribution (using the vacancy method) to activate the melting process is represented through the modeling of the AlLi (B32) phase, which is an ordered solution with a wide solubility range according to classical thermodynamics. Finally, the trustworthiness of all proposed methods to predict the melting behavior, including solidus and liquidus lines of the Al-Zn system is discussed. Ultimately, a series of practical recommendations for classical MD modeling is provided in the conclusions section.

2. Classical Molecular Dynamics simulation methodology

A series of classical MD simulations were performed to explore the efficiency of the vacancy/void method [52] , the interface method [59] and the grain method for the determination of the melting temperature of a range of solid metallic phases, i.e. pure metals, congruently melting intermetallics, peritic intermetallics, as well as ordered and disordered solid solutions. The interface method is typically more complicated to implement than the void method which is commonly used to evaluate the melting temperature of a supercell [53, 54]. Other methods exist but were not used in the present work. As an example, the temperature hysteresis method, proposed by Luo et al. [72] consists in imposing a cyclic heating ramp followed by a cooling ramp on a given supercell while reaching both overheating and undercooling conditions. This methodology allows a more precise evaluation of the melting temperature of pure metals. However, as reported by Zou et al. [54] this method is not reliable for the evaluation of the melting behavior of binary systems and was not considered here. The direct evaluation of the individual Gibbs energy of the solid and liquid phases as a function of temperature (via the thermodynamic integration method for example) is the most direct technique to obtain the melting temperature of a given solid structure [54], but for multicomponent systems, which require an accurate description of configurational entropy contributions, this method is difficult to implement [54]. Finally, Jess et al. (2000) reported a proper estimation of aluminum's melting point using the Gibbs-Duhem integration method [73]. Unfortunately, this approach requires the reparametrization of the interatomic potentials. In this work, methodologies for the melting point are instead studied using force fields trained with elastic and thermodynamic properties (ie., the training set does not include the melting point). [74, 75].

Table 1: Literature review on various MD approaches to evaluate the melting temperature, along with their implementation details.

Method to melt	Method to quantify melting	Details on simulation setup, study of convergence and evaluation of errors
Interface method [62]	No mention	No detail given on simulation setup for melting point evaluation, no mention on convergence nor evaluation of errors.
Void method [63], no mention on heating rate	Internal energy vs Temperature curve and Lindemann index	System sizes and structure provided, no specifics on voids other than their amount, no mention on convergence or error but melting plateau shown.
Void method [64], Heating ramp 2.5E+2K/ns	No mention	System sizes and structure provided, no specifics on voids other than their amount and them being randomly distributed, no mention on convergence nor evaluation of errors.
Perfect cell [65], Heating ramp 2.5E+7K/ns	Internal energy vs Temperature curve	Details on the ramp used but no specifics on cell creation, no mention on convergence nor evaluation of errors.
Interface method [66]	NPH run	Some detail on simulation setup, no detail on simulated cell, system size or geometry, no mention on convergence, provides error bar without context for its origin.
Perfect cell [67], Heating ramp 1K/ns	Internal energy vs Temperature curve	Reference structure and size of cell provided, no information on final geometry, no mention on convergence nor evaluation of errors.
Interface method [68]	NPH convergence	System sizes given without specifying used structure, mentions using convergence but doesn't display results, shows 95% confidence on some results.
Void method [61], NPH run instead of heating ramp	NPH run	Reference structure and size of cell provided, details on void size and geometry given, no mention on convergence, error mentionned but no values shown.
Perfect cell [69], Equilibration at a given temperature	Loss of long range order in RDF curve	Reference structure and size of cell provided, no information on final geometry, no mention on convergence nor evaluation of errors.
Interface method [70]	NPH run	Some detail on simulation setup, no detail on simulated cell, system size or geometry, no mention on convergence, error mentionned, no values shown.

For the vacancy method, we explored the effect of the initial ordering/distribution of defects/vacancies on the thermal stability of the solid lattice. The effect of this defect distribution introduced in the initial configuration of a multicomponent system is of high importance as energy barriers coupled to relatively short simulation times prevent the exploration of the complete phase space accessible to the system for some imposed temperature and pressure conditions. Additionally, we controlled the local chemical ordering surrounding a vacancy in multicomponent systems to study its impact on the energetic stability of the solid structure. The following list of structures were studied in our work via the void method: 1) pure metals (unary systems): FCC-aluminum 2) binary intermetallic compounds: Al_3Zr ($L1_2$, $D0_{23}$ ordered structures and FCC disordered phase), the ω-phase Al_4Cr [71], B32-AlLi and 3) disordered binary solid solutions: Al-Zn FCC-disordered (90 at.% Al). The results of the void method were systematically compared to those obtained using the interface method in pure systems. The latter was also applied to the exploration of the entire Al-Zn phase diagram to determine if classical MD simulations can directly evaluate the solidus/liquidus of binary phase diagrams. Finally, we completed our series of MD simulations by constructing nano-grains supercells for the Al-10Zn system to quantify the effect of the grain size on the evaluation of their melting temperature. The strength of the metallic interactions in all our MD simulations was classically described via the modified embedded atom model with the second nearest neighbor approximation (2NN-MEAM) [38, 42]. Interatomic potential parameters for pure elements (Al, Zn, Cr, Zr and Li) and for the binary Al-Cr and Al-Zr (derived from the Zr-HCP-allotope) systems were obtained from the literature [38, 41, 40, 76, 37, 77, 37], while the binary interactions for Al-Zn, Al-Li and Al-Zr (with Zr-BCC reference) were built in-house (section 9. Appendix), the potential parameters using the 2NN-MEAM formalism can be found in tables 3 and 4. Potential validation proofs are shown in the Electronic Supplementary Information (**ESI**). The potential parameters describing the force field according the 2NN-MEAM formalism were built by aiming to reproduce the calculated lattice parameters, bulk modulus, cohesive energy and elastic constants, without any consideration towards the melting temperature. To create this potential, the bulk modulus, the cohesive energy and the average equilibrium interatomic distance of the reference structure at 0K are set to the value obtained by DFT simulations. Then, both minimum and maximum cutoff parameters (C_{min} and C_{max}) are adjusted via a force matching method to simultaneously minimize the difference between the calculated elastic constants and lattice parameters by DFT and with the 2NN-MEAM potential at 0K.

2.1. Classical MD simulation details

All our classical MD simulations were performed with the LAMMPS package [78]. Each supercell representing one of the crystal structures listed in table 2 was created using atomic position files provided by the Material Project [79]. Firstly, these supercells were relaxed and equilibrated at null pressure and 300K for 0.11ns using a timestep of 1 femtosecond. A heating ramp was then started by performing incremental isothermal/isobaric runs of 0.11ns until reaching a maximal temperature (which was adjusted based on the experimental melting point of each studied system). The first portion of the isothermal/isobaric MD run (i.e. 0.01ns) was required to equilibrate the supercell while the rest of the simulation time (i.e. 0.1ns) was used to evaluate the averaged thermodynamic properties of the supercell. A phase space exploration of 0.1ns was found to be long enough to reach ergodicity. Temperature increments were varied from $50K$ to $5K$ as the temperature approached the melting point of the structure. Error bars for each thermodynamic property were evaluated from the average and standard deviation of the MD data obtained during the 0.10ns sampling period. A Nosé-Hoover thermostat/barostat [80, 81] was used in all our simulations; periodic boundary conditions (PBC) were systematically applied. The effect of the cooling rate on the solidification was explored in a previous study [37].

Fig. 2 shows an example of such a heating ramp for the evaluation of the melting temperature of an FCC aluminum supercell. It can be noticed that the enthalpy curve varies linearly as a function of temperature up to the melting point where a sharp enthalpy increase occurs as a result of this first order transition. Complementary MD simulations presented in fig. 3 were conducted using constant heating rates instead of our proposed heating strategy. These MD simulations did not show any significant

Table 2: Crystal structures and sizes of the supercells used in the classical molecular dynamic simulations melting experiments.

System	Al	Al_3ZrL_{12}	$Al_3ZrRandom$	Al_3ZrD0_{23}	Al_4Cr	$AlZn$	$AlLi$
Crystal Structure	FCC	L_{12}	FCC	$D0_{23}$	$\omega-phase$[71]	Random FCC	B32
Size $a*b*c$	$10*10*10$	$10*10*10$	$10*10*10$	$10*10*3$	$6*4*6$	$10*10*10$	$7*7*7$
Number of atoms	4000	4000	4000	4800	5104	4000	5488
Materials Project ID [79]	134	569775	569775	365	Not applicable	134	1067
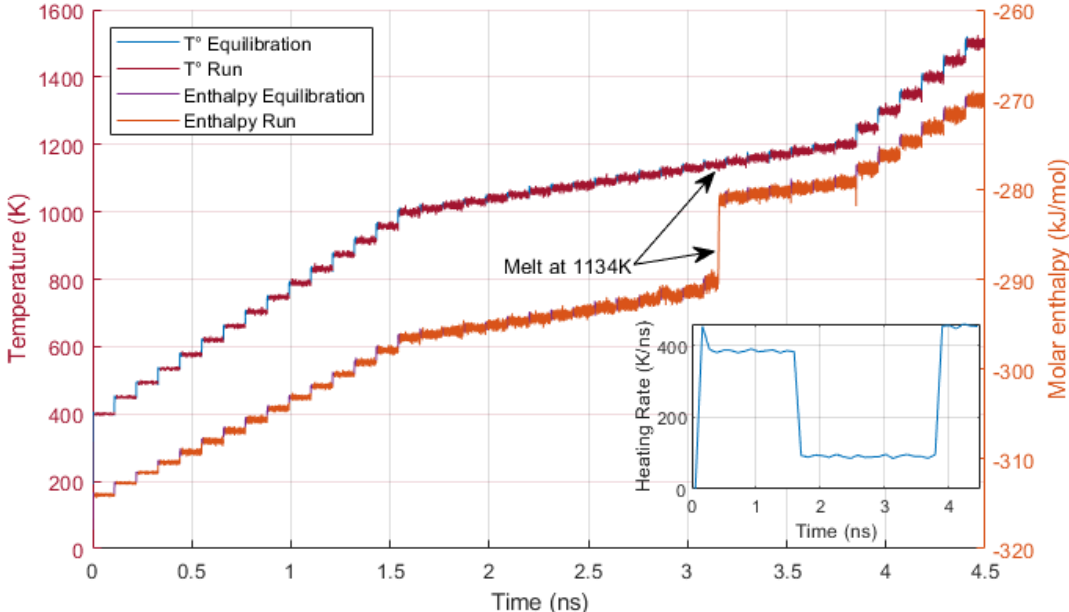
Figure 2: Variable heating ramp in MD to simulate the melting of a pure FCC aluminium supercell of 4000 atoms without vacancies. Inset panel shows the evolution of heating rate as a function of time. Jump in enthalpy is associated with first-order phase transition.

deviation in the evaluation of the melting temperature while requiring significantly higher simulation time, being more computationally costly. Similarly, we tried replica exchange MD using the *temper/npt* function, which also showed no increase in accuracy at a significant increase of computational cost. This method works by swapping the temperature of parallel runs of the same simulation to avoid an undesired phase change to occur, and to happen at the moment the different parallel runs would aim to change phases. This method was used in the past to help break the superheating/undercooling effect [82].

The size of each supercell was adjusted based on a series of MD simulations presented in Figure 4. We see that the predicted melting temperature of a FCC aluminum supercell reaches a constant value above a supercell size of 2000 atoms. Supercells containing at least 2000 atoms but generally about 4000 atoms were used in all our simulations to ensure an accurate evaluation of the melting temperature while limiting the computational cost of each numerical experiment (which was already quite high due to the total time required to apply the heating ramp as seen in Figure 4). The exact number of atoms for each supercell (which is a function of the primitive cell of the studied crystal structure) is reported in table 2.
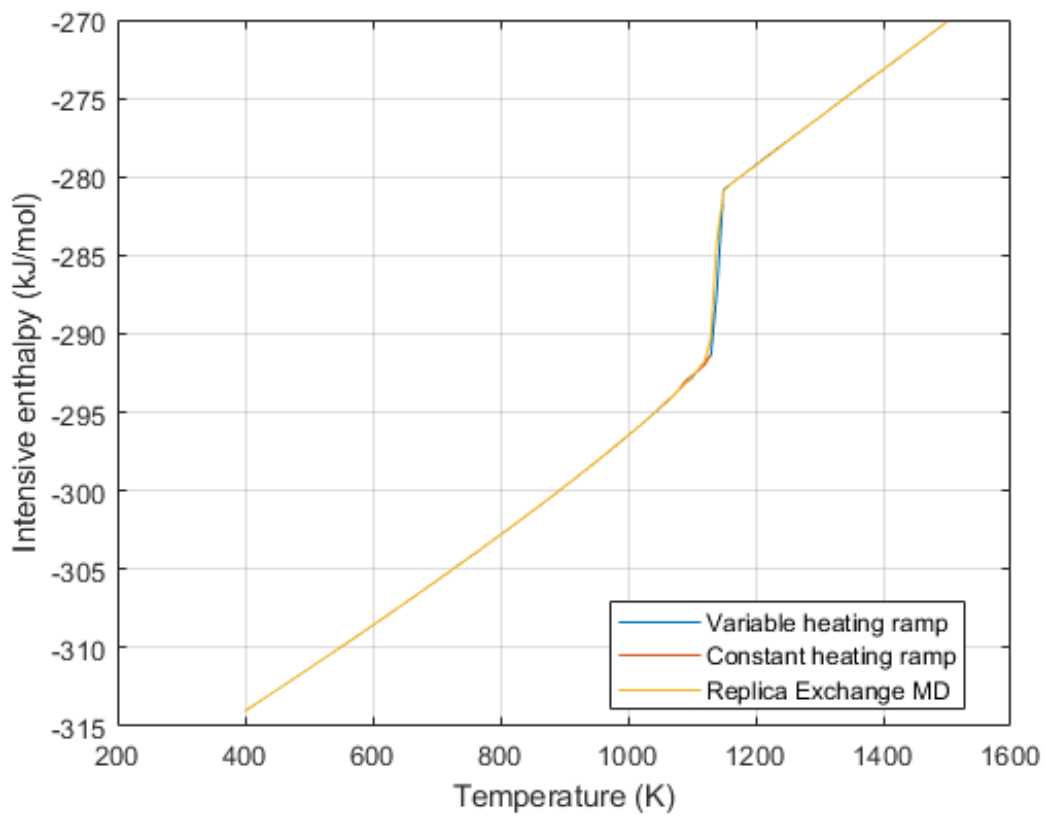
Figure 3: Comparison of methodology to induce melting in a pure aluminum lattice without any vacancies. Computational costs of each method were of; 80 CPU-hours for the variable heating ramp, 260 CPU-hours for the constant heating ramp, and 1020 CPU-hours for the replica-exchange MD method.
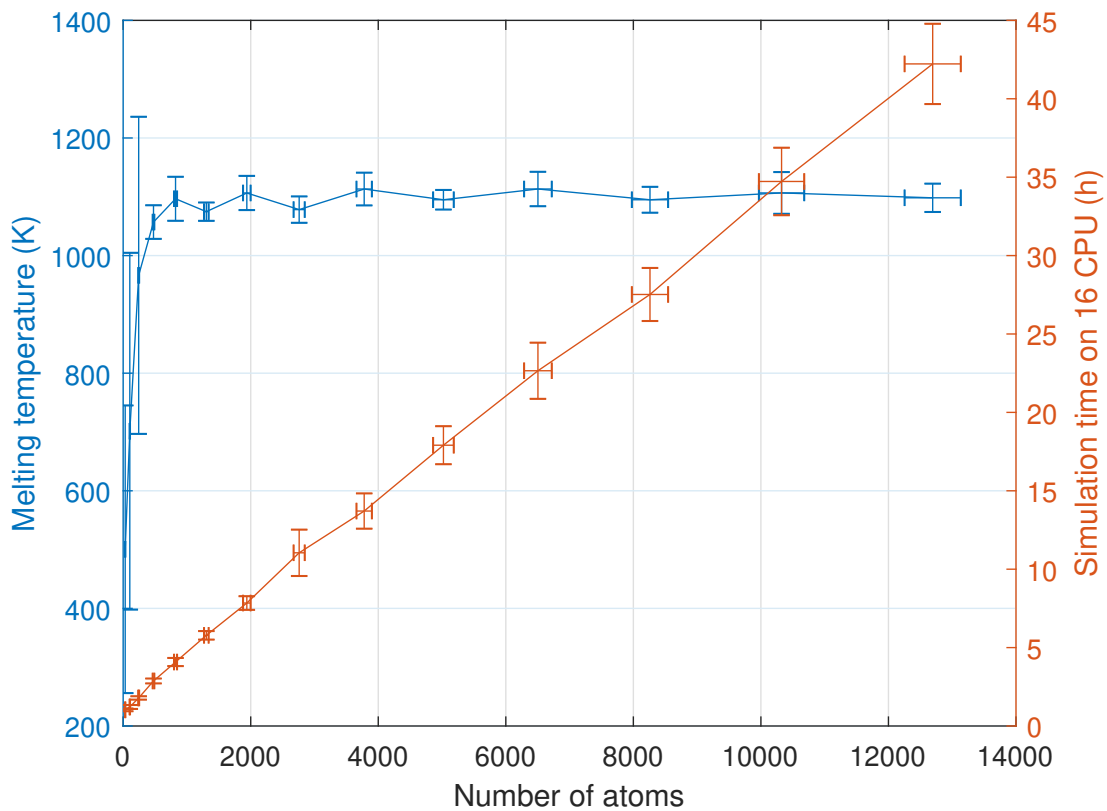
Figure 4: Impact of the simulation size on the melting temperature prediction (blue) and its associated simulation time (orange). 11 runs were performed for each system size on pure FCC aluminium cubic supercell with and without vacancies, i.e. 0, 0.5, 1, 1.5, 2, 3, 5, 6.5, 8, and 10 % of vacancies. Runs were averaged, and error bars stand for the standard deviation. Vacancy samples are included to display the resulting variability in results when accounting for their presence.

2.2. Melting criteria

Different criteria were employed to evaluate the melting temperature of a supercell. These are, in order of importance, 1) the enthalpy curve method, 2) the Lindemann index method and 3) the radial distribution function analysis. In the enthalpy curve method, we simply tracked the occurence of an enthalpy jump as a function of temperature. For comparison purposes, the Lindemann index (q_i) was also calculated to evaluate the melting temperature of the studied systems, it is defined via the following equation [83]:

$$q_i = \frac{1}{N-1} \sum_{j \neq i} \frac{\sqrt{\langle r_{ij}^2 \rangle - \langle r_{ij} \rangle^2}}{\langle r_{ij} \rangle} \tag{1}$$

Where r_{ij} is the distance between atoms i and j, N is the total number of atoms in the simulated cell, and the brackets $\langle \rangle$ indicate time averaging at a given temperature. This adimensional index computes the individual atomic mobility through an indirect measurement of the mean-square displacement (MSD). A transition from a solid to a liquid state induces a sharp increase of this index as the long range symmetry of the solid is destroyed, allowing much more mobility to the atoms in the liquid state.

Figure 5 shows the application of method #1 and #2 to the evaluation of the melting temperature of an FCC aluminum supercell. It confirms that both the enthalpy jump and the Lindemann index jump occur at the same temperature. It is to be noted that the Lindemann index evaluation is computationally expensive when compared to the direct enthalpy method. Because of the lower computational overhead, the enthalpy method was used in most cases and was confirmed with the Lindemann index when necessary (i.e. due to unique structures or melting dynamics impacting the enthalpy curve).

2.3. Detailed description of the MD melting/solidus evaluation methods

2.3.1. Vacancy/void method

It is known that a defect-free lattice mechanically melts at a much higher temperature than its experimental value in classical MD simulations. One basic approach to estimate the true melting temperature (T_b) is to simply convert the perfect-lattice melting temperature (T_t) via the thermo-statistical relationship proposed by Belonoshko et al [86], which is defined as follows:

$$T_b = \frac{T_t}{\frac{ln(2)}{3} + 1} \tag{2}$$

A more thorough approach is to introduce defects in the simulated supercell. The conventional void/vacancy method is well documented [52, 53, 54]. It is the most used MD methodology to rapidly assess the melting temperature of solid structures. Previous works indicated that the void size distribution was not a critical parameter when simulating the melting of argon solid structures [52]. A plateau of the melting temperature as a function of vacancy concentration was also proposed [52]. The implementation of this method is simple in comparison to other methods presented in this paper. Many strategies can be used to introduce vacancies in an initially perfect solid supercell. It is to be noted that few studies in the literature carefully study the effect of the initial configuration on the results of such classical MD simulations, although it is of fundamental importance and at the heart of high quality simulations [13]. The simplest approach is to randomly remove a specific number of atoms to generate an initial configuration to be melted. The generation of such random initial configurations should be repeated several times in order to evaluate more precisely the melting temperature of a structure with a given concentration of vacancies. It is important to note that these new methods have the goal of reducing the activation energy to melting in a dynamic process, and can require a high vacancy concentration. The danger of this method is reducing so many atoms that their removal and following restructure will cause a variation of the lattice's cohesive energy. In our work, atoms were removed from solid supercells in order to have an atomic concentration of vacancies ranging from 0% to 10%. In many metals and alloys, such a high concentration of vacancies is never experimentally
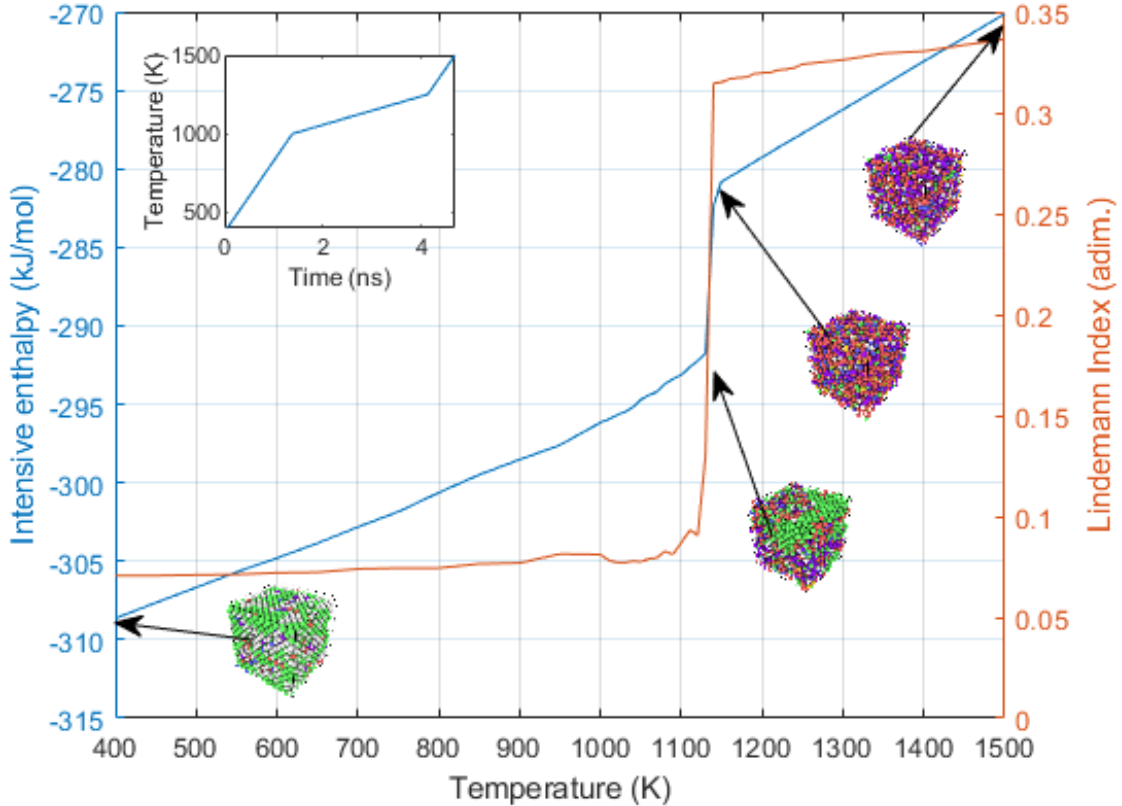
Figure 5: Comparison of the enthalpy method and the Lindemann index method for the evaluation of the melting temperature of a FCC aluminum supercell upon heating and cooling. Colors in the supercell structures are a filter showing local order, which was computed using the Polyhedral Template Matching (PTM) analysis [84] implemented in Ovito [85]. Green is used to identify aluminum atoms with an FCC local ordering. The change of color from green (FCC) to blue (BCC), red (HCP) and yellow (ICO) is an indication of local melting.

reached. Therefore more vacancy configurations were generated for concentrations below 3%. Moreover, we found that higher concentrations of vacancies didn't have a noticeable impact on the resulting melting temperature (which started to plateau and then numerically fail by collapsing into itself above this concentration). As it will be presented in this work, the melting mechanism of solid supercells in classical MD strongly depends on the local structure of vacancies within the crystal structure. In order to better understand and quantify this effect, we considered the creation of four different types of vacancy structures, i.e. random vacancies, perfectly-ordered vacancies, splitting-void vacancies and single-void vacancies. In the last two approaches, vacancies are clustered to generate a single large void within the supercell. Fig. 6 displays an example for each type of vacancy structural arrangement for a vacancy concentration of about 10% (atomic). A brief description of each approach is presented below:

Random vacancies method
An example of such a random vacancy distribution is presented in the upper left panel of figure 6. All the trend-lines obtained from this method will show error-bars because of the random nature of the approach. The LAMMPS's `delete_atoms` function using distinct seeds to randomly choose the sites of the lattice to remove atoms was used. Each vacancy concentration simulation was run 11 times to quantify the uncertainty associated with the simulations of of randomly distributed vacancies. For high-order systems, the total computational cost to evaluate the error of each simulation was too high
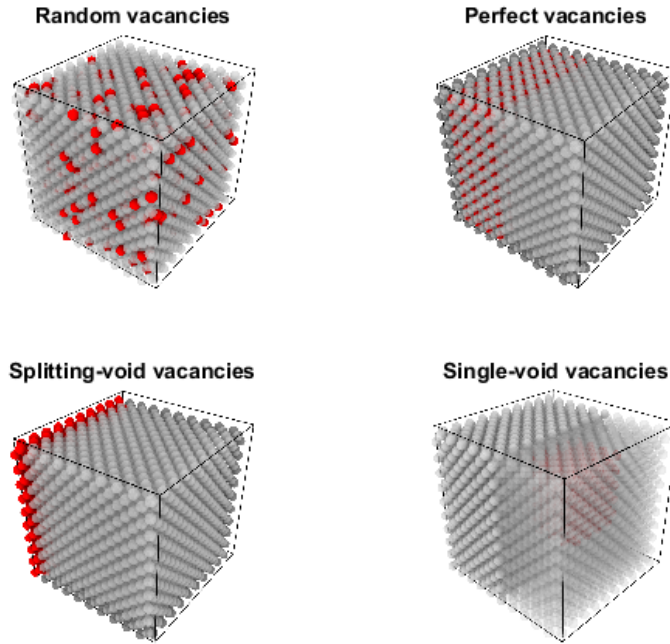
Figure 6: Visualisation of vacancy distribution for pure FCC-Al 10x10x10 lattices, red particles total 10% of their respective simulation's total number of atoms and are deleted when simulation starts, generating vacancies.

to systematically quantify their uncertainty.

Perfectly distributed vacancies method
In this approach, specific atomic sites are periodically targeted until the vacancy concentration is reached. This results in a perfectly ordered vacancy lattice as presented in the upper-right panel of figure 6. The goals of this method were to avoid the presence of di-vacancy defects and to precisely control the local atomic environment in the supercell.

Splitting-void vacancies method
This method consists in creating an infinite void of a specific thickness in the initially perfect supercell. This is done by removing entire layers of atoms in order to reach both sides of at least one boundary layer as presented in the lower left panel of figure 6. This way, the void is infinitely spread through this boundary layer. Such a configuration leads to the creation of two surfaces with atoms having a fraction of their original nearest neighbors while the local ordering of the bulk atoms remain unchanged. This creates first and second nearest neighbors vacancies for the atoms near the surface of this void.

Single-void vacancies method
The single-void method is very similar to the previous splitting-void approach. The main difference is that the prism-shaped void is created within the bulk supercell far from its boundary layers as shown in the lower right panel of figure 6. This void will always be in the same shape as the domain, since most domains are cubic, the single-void is also in a cubic shape. This way, the single void which creates six distinct surfaces within the supercell replicates itself periodically via the imposition of periodic boundary conditions in all directions.

The direct consequence of the application of these different methods to introduce vacancies/void is an increase of the internal energy of the simulated lattice when compared to the perfect lattice. The sum of simulations launched using these vacancy application techniques cost approximately 60 core-years.

2.3.2. Interface method

In the interface method, a liquid supercell is put in contact with a solid supercell that propagates in the solid or liquid part of the merged supercell as a function of the imposed temperature. As reported in the literature for many systems [53, 54], the melting front can rapidly propagate without requiring atomic diffusion because of the rapid destruction of the long range order symmetry via a sum of local atomic rearrangement. In this work, the simulation setup works by creating a solid rectangular prism simulation box. Then the entire simulation box is heated to the target temperature. At this stage, half of the simulation box is heated far above the melting temperature via NPT simulations. In this region of the simulation box, the supercell is allowed to equilibrate/relax its volume via lattice contraction/expansion in the direction perpendicular to the interface only. Once melted, this region is brought back to the same temperature. The entire simulation box is finally equilibrated over a long simulation time of 1.0 ns [60]. This process is performed at multiple temperatures in order to evaluate the melting temperature of the system. This setup of the simulated interface is the main difficulty of this approach. The splitting of the simulation box into two distinct regions causes a discontinuity in the periodic boundary conditions. A finely tuned approach is required to avoid numerical instabilities that would prevent the construction of an interface in equilibrium. Running the sum of these simulations cost approximately 40 core-years.

2.3.3. Grain method

The concept of this method is to mimic typical microstructures of metals and alloys which often feature equi-axed grains, such simulations have been previously used to try to give new applications to nanoalloys [87]. In this case, grain boundaries are the planar defects that promote the mechanical instability at the origin of melting. Examples of such nano-grains structures are presented in Fig. 7 for FCC Al-10Zn structures. Zn atoms were randomly distributed throughout the lattice with no consideration on their location relative to the created grain boundaries. These nano-grains supercells were created using a Voronoi tesselation method implemented in the QuantumATK R-2020.09-SP1 software [88]. This grain method is computationally intensive due to the very high number of atoms which is required when increasing the size of the grains (the highest system size reached 13 millions atoms in our simulations). As it will be shown in section 3.2.4, the increase of the grain size leads to a higher melting temperature of the system until a plateau temperature is reached which is in agreement with the previous experimental findings of Noori et al. [48] for pure FCC aluminum. Series of isothermal/isobaric MD simulations for 1ns were performed to identify the melting temperature of each solid structure. It was important to start each isothermal/isobaric MD simulation with the same initial grain structure as grain coalescence occurred in many cases, which led to the formation of a perfect lattice before its melting. Launching those simulations cost cumulatively approximately 80 core-years.

3. Results and discussions

3.1. Numerical melting of pure metals

3.1.1. Al-FCC

The first metal that was numerically melted with the methodology presented in section 2.1 is aluminum in its face-centered cubic structure. Its accepted experimental melting temperature is 660.5^oC (933.65K) [89]. Fig.8 shows the evolution of the melting temperature of simulated Al structures as a function of the vacancy concentration for different melting methods. As a comparison basis, the
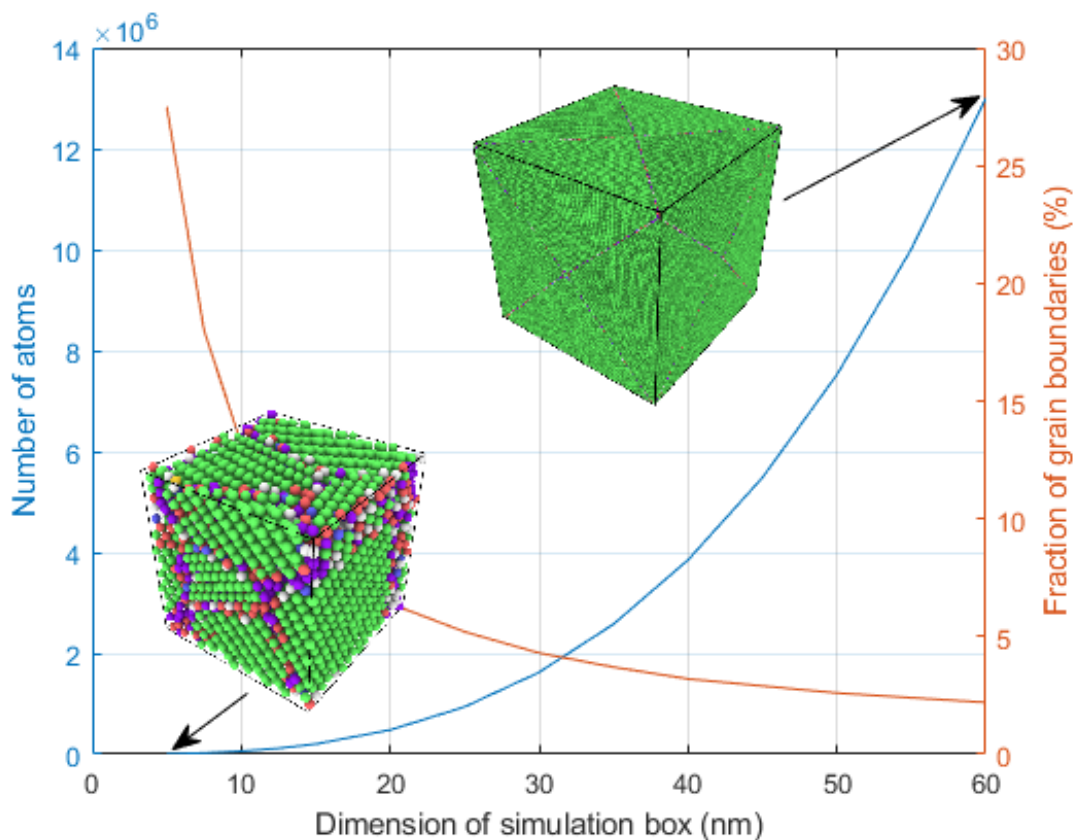
Figure 7: Creation of simulated cubic Al-10 at% Zn lattice with microstructural defects used to simulate results shown in fig. 14. Color in pictured lattices show local arrangement at lattice creation, green shows FCC, the grain arrangement of the lattice, the coloured areas in between FCC grains being grain boundaries. The bigger the dimension of the system the less grain boundaries are an important fraction of the lattice, with diminishing returns.

melting temperatures obtained from 1) a critical CALPHAD assessment, 2) the thermodynamic equation formulated by Belonoshko et al. (i.e. application of eq.2) and 3) the interface method are shown as horizontal lines. The virtually perfect agreement between the interface method and the assessed melting temperature is an indication of the quality of the parameterization strategy of the Al interatomic potential of Lee et al. [38]. The melting temperature of the perfect lattice without vacancies (i.e. 1135K) is presented as a star on this figure. The first striking feature is the wide variation of the melting temperature curve for the random distribution method. The evaluated melting temperature decreases up to a concentration of about 3% of vacancies, after which the melting temperature increases again to values close to the perfect lattice melting. A similar behavior is obtained for the perfectly ordered vacancies method. This trend is explained by the dissipation and agglomeration of vacancies originally introduced in the supercell at 0K via a local rearrangement of atoms which energetically stabilizes the supercell. This local atomic rearrangement is energetically favored above a certain vacancy concentration which increases the mobility of atoms within the supercell. The vacancy clustering effect induces an almost-linear increase of the molar volume as a function of the vacancy concentration as seen in figure 8. These volumes were taken from the results of randomly distributed vacancies simulations. Results show that the vacancy concentration (alternatively the single-void size) only impacts the energetics of the solid state.
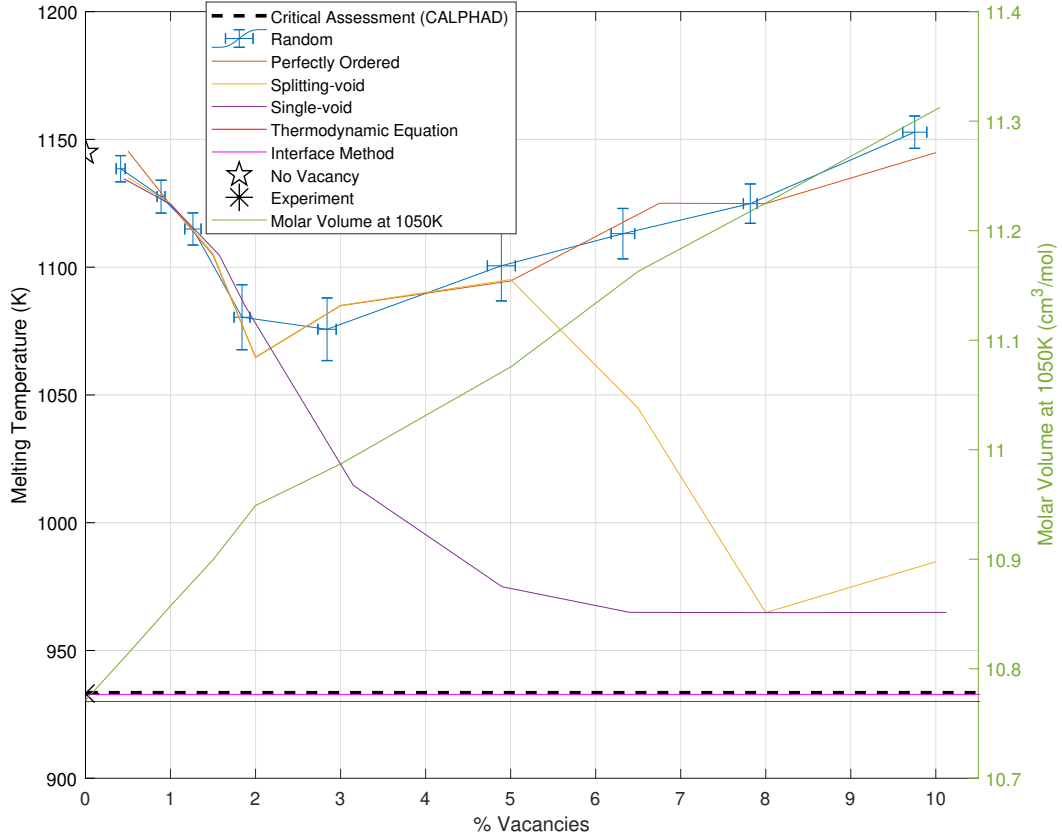
14

Figure 8: Melting behavior of pure Al-FCC as a function of the vacancy concentration (atom %) for different vacancy methodologies using an intially perfect supercell of 4000 atoms. The y-axis on the right shows the evolution of the molar volume of the supercell at 1050K as a function of the vacancy concentration for the random voids method. Experimental result taken from [90].

3.2. Numerical melting of binary metallic solids

This section presents the application of different MD melting approaches to several types of binary solid structures such as congruently melting and peritectically melting stoichiometric compounds, as well as partially ordered and disordered solid solutions. Moreover, we attempted to predict/evaluate the liquidus and solidus lines for an entire binary phase diagram (Al-Zn) via the interface method. Finally, we explored the grain method for the representation of the melting of an Al90-Zn10 FCC-disordered solid solution. In the case of binary compounds, it is important to mention that the introduction of vacancies shifts the chemical composition of the system unless specific rules are applied to stoichiometrically remove atoms in the supercell. For intermetallics accepting large quantities of defects (such as the AlLi-B32 phase), vacancies may also occupy preferential sites or may be randomly distributed in the structure. Therefore, we provided the resulting chemical composition of the supercell when required. We also explored the introduction of vacancies on specific lattice of these crystal structures.

3.2.1. Congruent melting intermetallics: Al_3Zr-$D0_{23}$/$L1_2$/Disordered-FCC

The melting behaviour of the Al_3Zr compound in the $D0_{23}$ (thermodynamically stable) and $L1_2$ (metastable) structures as well as in its FCC disordered state has never been systematically studied in
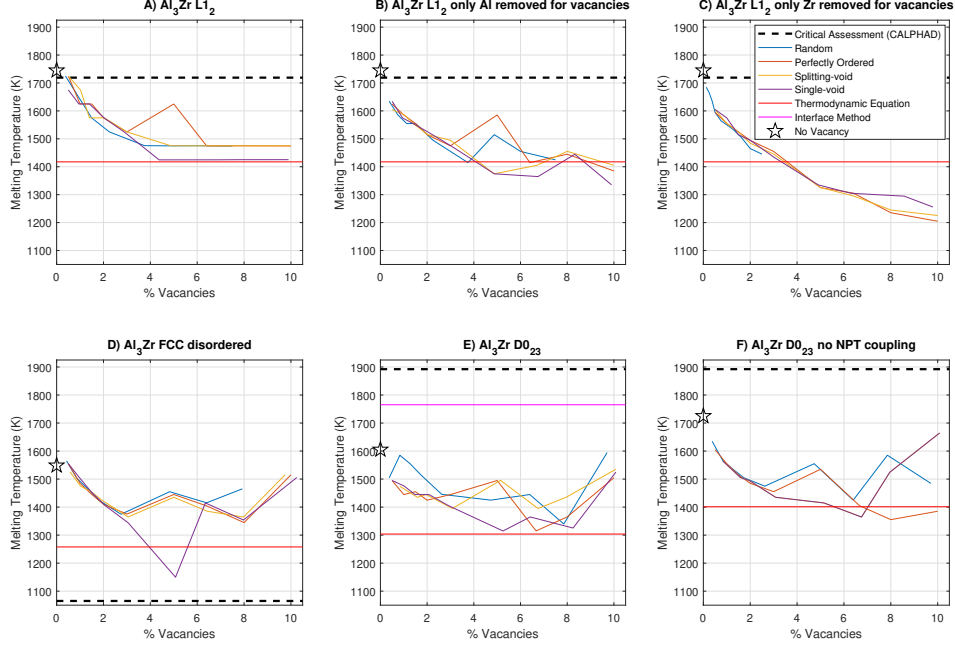
Figure 9: Melting temperature evaluation of Al_3Zr compounds (with the $L1_2$, $D0_{23}$ and FCC disordered structures) using the vacancy method for supercells containing between 4000-4800 atoms (see table 2). Experimental result taken from [91].

classical molecular dynamics. The available atomistic studies which explored the energetic behavior of this compound in the context of alloy solidification [92], heterogeneous nucleation [93, 94] and property evaluation [95, 96] were mostly performed through first principle calculations or MC simulations. When precipitation of the Al_3Zr compound occurs, it has been found that studying its behavior is challenging due to its heterogeneous nucleation at low supersaturation while high supersaturation cannot be achieved due to its nature, the stable $D0_{23}$ structure is the only Al_3Zr structure that precipitates if it is given enough annealing time [94] while the $L1_2$ structure requires a lower treatment temperature and holding time [97]. The evolution of the first-nearest neighbor fractions for each structure (before and after the introduction of vacancies) used in our simulations is reported in table **??**. Fig. 9 compares the melting temperature using the vacancy method of Al_3Zr in the $L1_2$ (panels A,B and C), $D0_{23}$ (panels E and F) and FCC-disordered structures(panel D) starting with perfectly ordered supercells as described in table 2. Experimental results have shown that in both the $D0_{23}$ and $L1_2$ phases, defects are uncommon and most commonly planar defects [97]. A striking feature of these melting curves is that the introduction of random vacancies within the lattice of the ordered Al_3Zr-$L1_2$ structure drastically lowers its melting temperature. The predicted melting temperature of the perfect lattice (0% vacancy) is in fact already close to the melting temperature obtained from computational thermodynamic calculations performed with the FTlite database of the Factsage software (i.e. about 1720K). These are clear indications that this solid structure is significantly destabilised by vacancies which is in agreement with the stoiochiometric nature of this line compound [98]. Two supplementary series of MD simulations were performed to analyze how the introduction of vacancies on specific lattice sites modulates the melting temperature of this structure. At low vacancy concentration (i.e. below 3%), the preferential removal of Al (panel B) and Zr (panel C) leads to similar melting temperature depletion. Above this concentration, the removal of Zr atoms within the supercell has a more pronounced effect on the melting temperature than for the removal of Al atoms. The evolution of the

melting temperature of the Al_3Zr FCC-disordered solid solution (panel D) is not too impacted by the introduction of vacancies even up to concentration as high as 10%.

The Al-Al bonds are much weaker than the Al-Zr and Zr-Zr bonds (which are the strongest interactions in this compound). The removal of Zr atoms (which are involved in the more energetic Al-Zr and Zr-Zr bonds) will naturally decrease the energetic stability of Al_3Zr compounds more than the removal of Al atoms (which are involved in the less energetic interactions). This figure also shows the distribution of 1NN interatomic distances which was obtained from a sampling of all the Al_3Zr structures (listed in table 2), from their perfectly ordered structures up to their solid state prior to melting (no special weighting functions used to favor some configurations). The average first nearest neighbor distance lies between the equilibrium interdistance of Al-Al and Al-Zr bond, skewing towards Al-Zr. This is explained by the high Al-Zr pair fraction for all the crystal structures of this compound Zr-Zr 1NN bonds are only present in the FCC disordered structure or in ordered supercells with high fraction of vacancies. This low pair fraction reduces the energetic impact of Zr-Zr bonds on the melting of these structures.

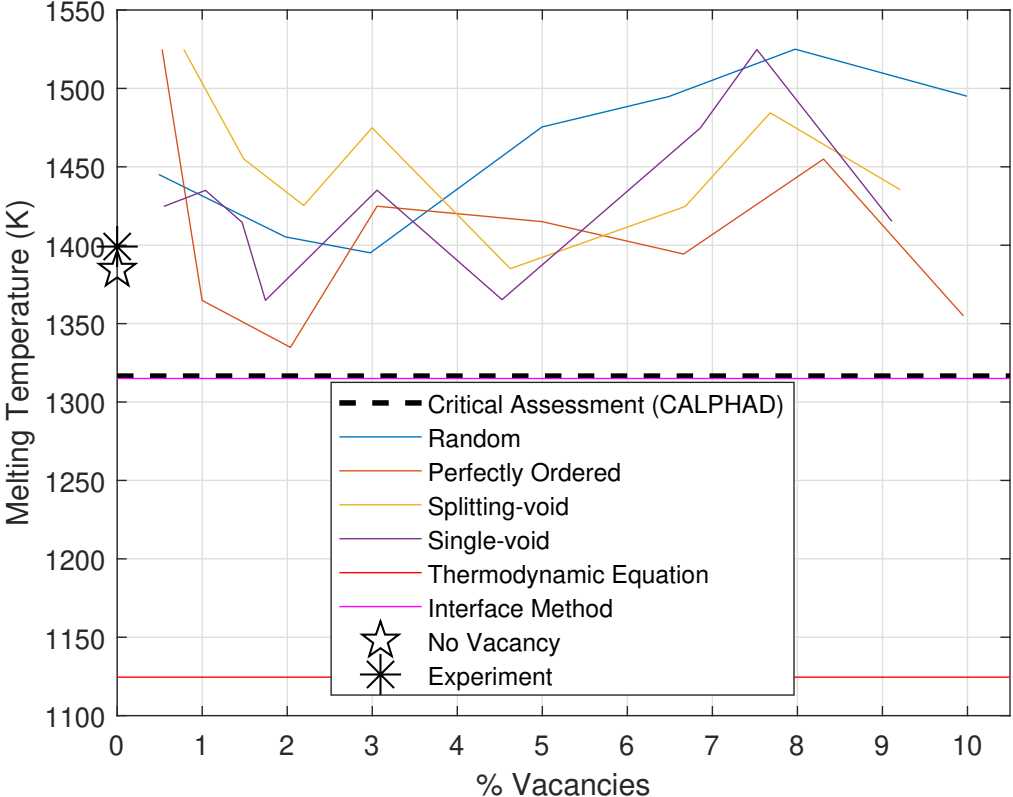### 3.2.2. Peritectic melting intermetallic: Al_4Cr

Figure 10: Melting behavior of pure Al_4Cr for different methodologies of applying vacancies with 5104 atoms. Experimental result taken from [99].

According to the work of Fan [71, 100], the ω-Al_4Cr phase is the most stable Al_4Cr phase at high pressure, transitionning from the μ-phase, a peritectically melting intermetallic [100, 101]. This stability was found to allow the structure to accept the presence of defects [71]. Fig. 10 shows the evolution of the melting temperature of this compound as a function of the concentration of vacancies.

Contrary to all the Al$_3$Zr ordered compounds presented in section 3.2.1, the melting temperature of the Al$_4$Cr intermetallic is not much impacted by the introduction of vacancies in its perfect structure. The melting temperature of the perfect lattice is lower than with vacancies,this is because the $\omega - phase$ [71] is unstable and the presence of vacancies allows it to restructure itself. This was confirmed with additional tests on the Al_4W structure (Materials Project id-30336) using the Al-Cr potential, which did not display this behavior. The interface method displayed the best prediction of the melting point because this method bypasses this structure's ability to accept lattice defects.

3.2.3. Ordered solid solution with a wide solubility range: AlLi-B32 solid solution
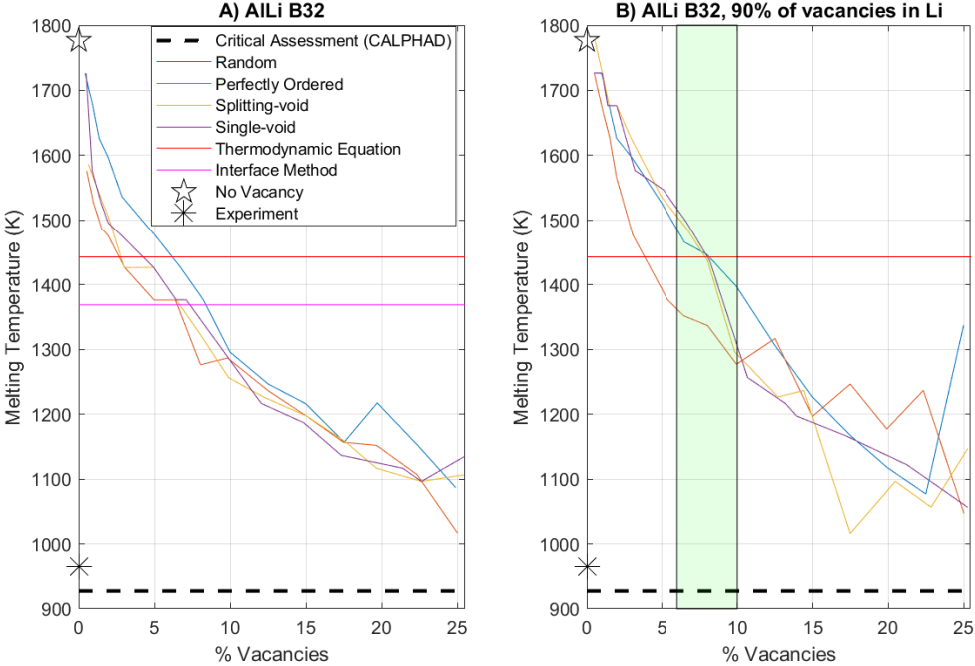

Figure 11: Melting behavior of pure AlLi for different methodologies of applying vacancies with 5488 atoms. Green section shows normal quantity of vacancies in the AlLi lattice in AlLi-B32 phase, which is mostly present in the sites where Li should be located. Experimental result taken from [102].

The AlLi phase has a B32 structure [103, 104, 105] and presents a large solubility range extending in both Li-rich and Al-rich composition at high temperature and mainly in the Al-rich at low temperature [106]. It is the stable phase that saturates the Al-FCC matrix at equilibrium. Under aging conditions typically imposed after a solution heat treatment and quenching steps, the Al$_3$Li-L1$_2$ phase which is coherent with the Al-FCC usually precipitates first. The energetic behavior of the AlLi-B32 phase is conventionally described via the compound energy formalism via a two-sublattice model. In this thermodynamic model, Al and Li are allowed to occupy the first sub-lattice while the second sublattice either hosts Li atoms or vacancies. The vacancy concentration at the congruent melting of the B32 phase is 6% (molar) while a maximum vacancy concentration of 10 % is calculated [107]. Fig. 11 confirms that the melting temperature of AlLi-B32 is underestimated by more than 100K when a perfect lattice is used in MD simulations. Two scenarios were explored in this figure for the introduction of vacancies: In panel A, vacancies were equally distributed between the Al and Li sites of the B32 structure while panel B shows the results of the simulations when 90% of the vacancies are introduced on Li sites. Vacancy concentrations up to 25% (molar) were tested in both scenarios since large fraction of these defects are experimentally observed for this structure. According to this figure, the site occupancy

18

of vacancies plays in important role to describe the melting of this solid solution. Indeed, the simulation results considering 90 % of the vacancies within the Li sites (Figure 11.B) indicates that most of the vacancy methodologies converge towards the thermodynamic melting temperature (black dashed line). The concentration of vacancies to be introduced in the supercell to reproduce the experimental melting temperature is more than the one calculated from our thermodynamic calculations (green shaded zone in 11.B). In fact, even the addition of 25% of vacancies is not sufficient to reach the experimental melting point of this intermetallic. The interface method considerably underestimates the melting point as the chemical environment for void sub-lattices is not integrated within that approach. Therefore, MD simulations must consider vacancies to properly describe solid solutions and to be consistent with their classical thermodynamic modeling.

3.2.4. Disordered solid solutions: FCC solutions of the Al-Zn system

Zinc is an essential alloying element at the heart of the development of aluminum alloys of the 7000 series [108, 109]. It has a maximum solubility of 16 wt. % at 374°C in the Al-FCC solid solution and forms intermetallics when Mg (such as the $MgZn_2$) and Cu are added to the alloy [110]. Al-Zn interactions are not energetically favorable when compared to Al-Al and Zn-Zn interactions which is at the origin of the immiscible behavior in the Al-rich side of the FCC solid solution. At high temperature, configurational entropy effects dominate and stabilize the presence of Zn in the Al-FCC disordered solution. Zn additions can go up to 10 % (by weight) in the 7000 series [111][112], which is the first composition we studied for this system in our work. The Al-Zn phase diagram being simply defined by three disordered solutions (i.e. the Zn-rich HCP, the Al-rich FCC and the liquid disordered solutions), we also explored in this section the possibility to obtain/predict the melting behavior for the entire composition range via the interface method considering both random and distinct chemical composition for the solid and liquid zone of the supercell. Finally, we complete this work by studying the effect of considering FCC grains of different sizes on the melting of an alloy containing 10 at.% of Zn.

Void method. Fig. 12 shows the evolution of the melting temperature of an Al90Zn10 (weight) disordered FCC solution. It shows that the single-hole vacancy method reaches the liquidus temperature obtained from FactSage thermodynamic calculations at a vacancy concentration of around 6-10%. The reduction of the melting temperature induced by the introduction of vacancies with our proposed strategies is similar to the one for pure Al-FCC at low concentration. At high vacancy concentrations, the stabilization of the supercell by vacancy agglomeration when using the random distribution method is not observed. The presence of non-energetically favorable Al-Zn and Zn-Zn interactions in the supercell are at the origin of this behavior.

Interface method. The possibility to obtain entire phase diagrams from series of classical MD simulations is attracting as it greatly reduces the amount of experimental work to be performed and provide access to melting properties of multicomponent systems. A recent study by Haapalehto et al. [114] presented the application of semi-grand canonical Monte Carlo (SGCMC) simulations to evaluate the liquidus and solidus lines in the Al-rich side of the Al-Cu binary phase diagram. This method involves the modulation of the chemical composition of the supercell for some imposed chemical potential to the Monte Carlo method to ultimately construct Gibbs energy curves. It is the most common method used to generate liquidus/solidus data of binary systems [115], but is highly sensitive to the interatomic potential used. Other recent studies proposed MD approaches based on the interface method to evaluate liquidus/solidus lines [116].

The Al-Zn system is a good benchmark example as its phase diagram shows phase equilibrium regions involving only disordered solutions, i.e. the FCC, HCP and liquid. Moreover, the enthalpy of mixing in the solid state presented in the supplementary material (**Fig. S3**) is slightly positive and is easily overcome by configurational entropy effects above 600K. Therefore there should be no chemical short range ordering favored during our MD simulations.

From a structural evolution and energetic perspective, the mechanism that leads to the melting of such multicomponent system is drastically different from the one for its solidification. As reported
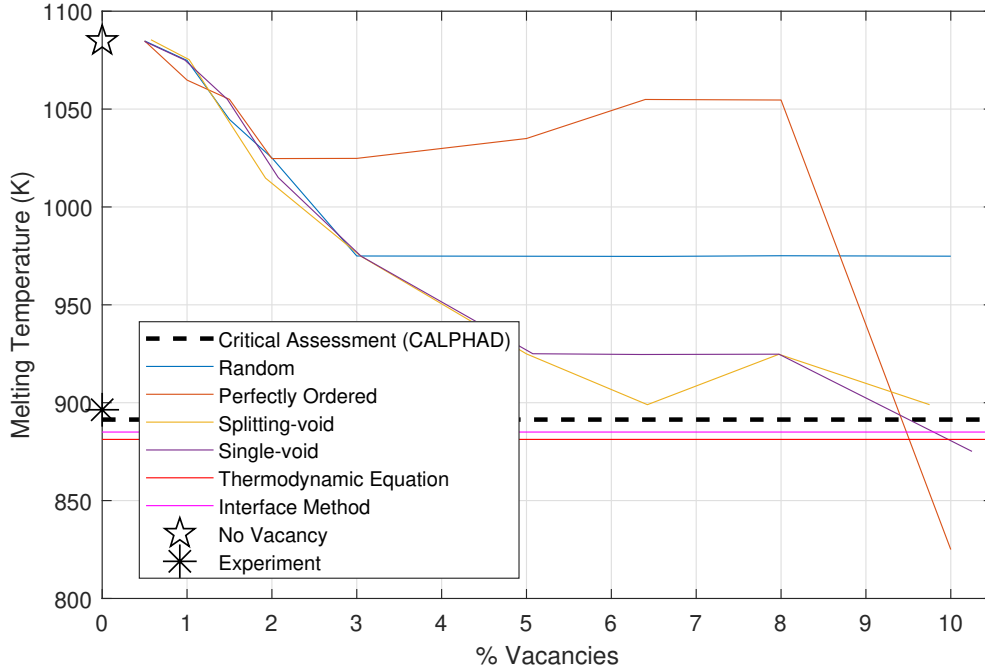
Figure 12: Melting behavior of FCC-disordered AlZn with 10% at. weight Zn, for different methodologies of applying vacancies with 4000 atoms. Dashed line represents the liquidus temperature. Experimental result taken from [113].

by Glicksman [117], melting can be viewed as a lattice vibrational instability that breaks the long range order symmetry almost instantaneously. This leads to the formation of a liquid phase of higher enthalpy than the parent solid structure. During solidification, local ordering of atoms can form aggregates of distinct composition which are precursors for the formation of solid structures of lower enthalpy. In MD simulations, it has been shown that local/medium ordering can ultimately lead to a complete solidification process without the occurrence of a complete first-order transition. In the interface method, melting is observed by the rapid progress of the solid/liquid interface toward the solid zone of the supercell. The diffusion being limited in the solid state (especially for perfect structures), it is difficult to reach local composition of the first liquid to form in conditions such as the one presented in Figure 13 (since there is no chemical driving force to obtain this distinct chemical composition). Therefore, MD simulations performed in order to obtain the melting properties via the interface method with an homogeneous composition for both the liquid and the solid will not allow the evaluation of the solidus of the system. At best, it provides a phase transition temperature close to the liquidus line above which the liquid that forms has the bulk composition of the system. To be able to evaluate both the liquidus and the solidus, distinct composition and weight fraction of the solid and of the liquid zones need to be considered. In this work, we explored the conditions provided by the calculated Al-Zn phase diagram obtained using the FTlite database of FactSage. The composition of the solid and liquid (as well as their weight fraction) for a system in the liquid-FCC 2-phase region were obtained from the phase diagram and used to construct the hybdrid supercell. The lattice parameter of the resulting simulated domain was scaled as a function of the composition based on a simple mixing rule using aluminum and zinc lattice constants in the FCC structure. Fig. 13 shows three distinct examples of the supercell constructed based on phase diagram data for a 50-50 at.% composition. The temperature range of the biphasic domain was split in 5 equidistant zones which allowed to modulate the fraction of liquid and solid in the supercell as well as their individual composition. The interface method as described by Watt et al. [60] was then applied. The results for both strategies are also

reported in figure 13. The traditional interface method involving the same composition for the liquid and the solid regions provides an evaluation of the liquidus line while the customized interface method with variable composition and phase fraction provides an evaluation of the solidus line. We believe this is because the adequately organized structure helped the simulation melt at a lower temperature that globally fit the solidus line. In our simulations, the analysis of the enthalpy, of the Lindemann index and simulation snapshots were used to determine the accurate temperature of the phase transition.
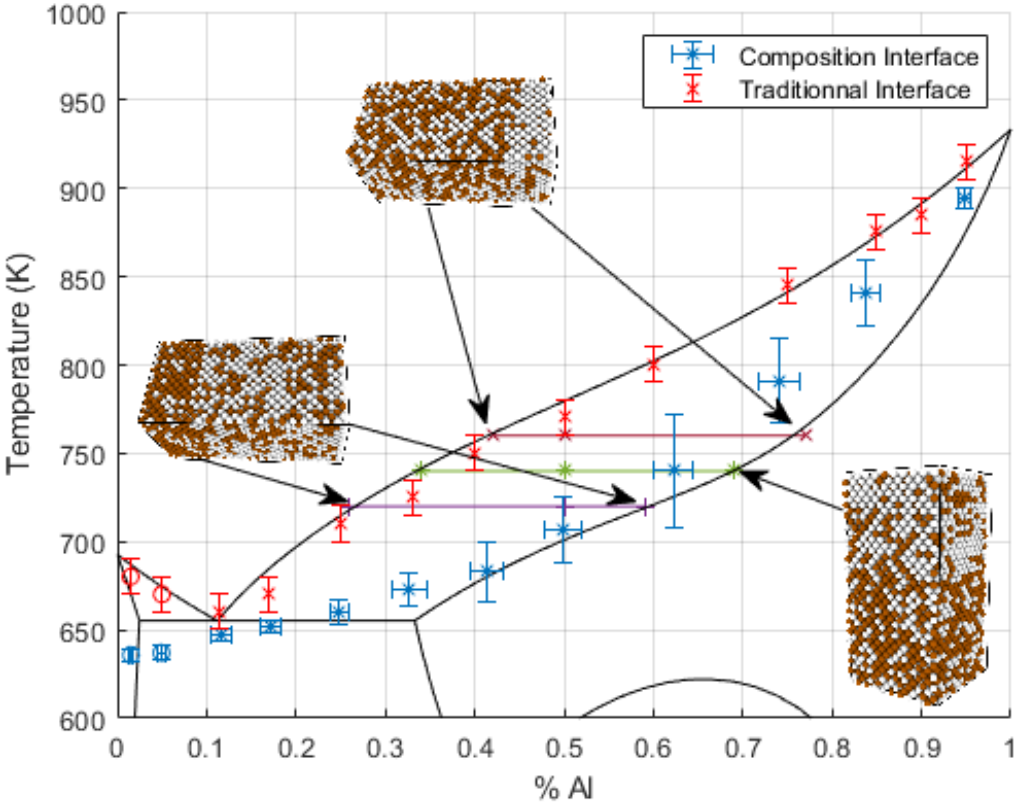
Figure 13: Creation of composition interfaces for an AlZn alloy at 50% Al globally. Grey particles represent Al atoms and brown particles represent Zn atoms. Each coloured bar shown is at a given temperature used to create the chosen system. Also shown are results of the simulation of the Al-Zn system with this composition interface methodology, compared to the same average compositions with the traditionnal interface method. Points with circle markers are marked differently to show they were created with an FCC microstructure despite theoretically requiring an HCP microstructure.
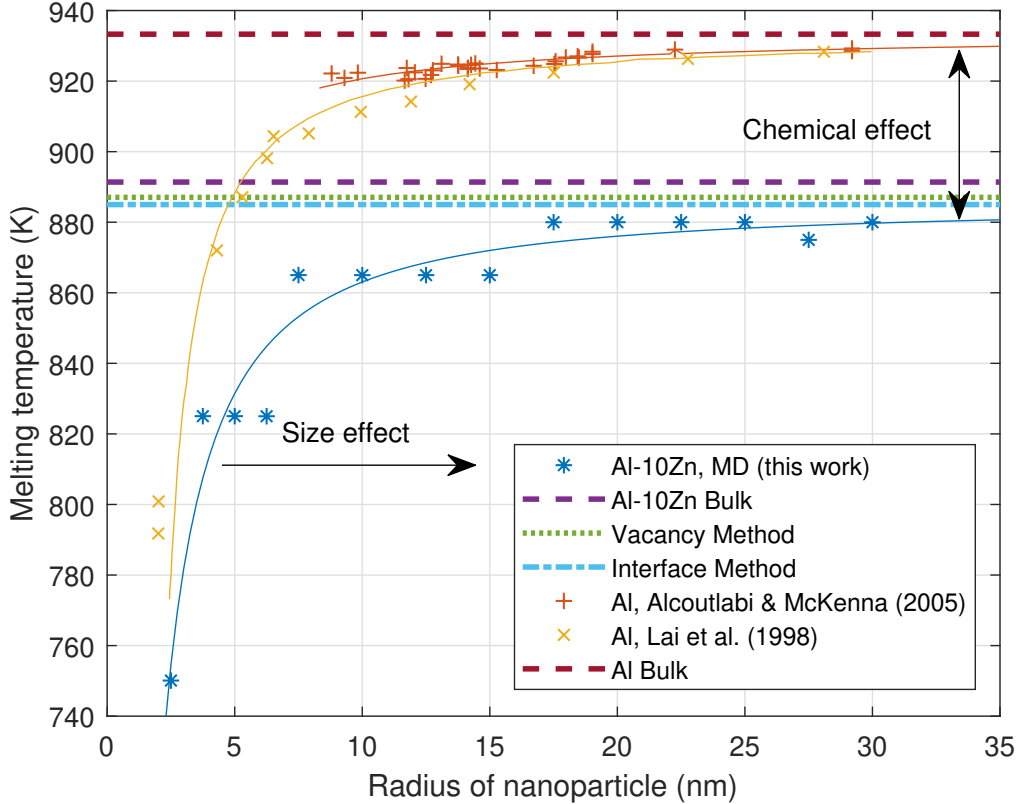
Figure 14: Results of simulating microstructural defects in Al-10Zn lattices. Compared with Al nanoparticles melting temperature at similar sizes. Every dataset (MD and experimental) is fitted and displayed, bulk melting temperatures for Al and Al-10Zn structures are displayed as horizontal lines.

Grain method. The last strategy used in our work to explore the melting in classical MD was linked to the creation of equiaxed nano-grain structures. Contrary to real macroscopic structures, we did not enrich grain boundaries with solute atoms (in this case Zn). We used instead homogeneous composition for each grain (including the grain boundaries). We therefore expected to predict the liquidus temperature for the imposed composition. Since the simulated lattices described in fig. 7 are of a single grain and neighboring grain boundaries when considering periodic boundary conditions, MD results were compared to nanoparticle melting temperatures. The grain size for the MD tests was programmed as an equivalent of the simulation size (l); therefore, the radius of grains was approximated as $l/2$ in Fig. 14. Figure 14 shows the evolution of the melting temperature of the supercell as a function of the size of the nanograins/nanoparticle considered in the simulations. Experimental results of melting depression for Al nanoparticles are also displayed in fig. 14. Al particles were chosen thanks to their similarity and due to a lack of data for Al-10Zn nanoparticles. Note that the melting temperature plateau that can be observed at different sizes are not the result of the melting dynamics like in previous simulations, but are the result of the incredibly high computational costs of this methodology, reducing the temperature resolution of simulations.

A closer inspection at the simulation dynamics revealed that melting began at the grain boundaries between simulated grains, which is in accordance with the known melting dynamics of experimental Al-Zn samples [118]. For grain radius (r) < 10 nm, the melting point is considerably reduced as the grain radius is decreased, this behavior is explained by the non-distinction of grains and grain boundaries at the nanoscale. By contrast, when r > 15 nm, the melting depression follows an equivalent trend as

the one experimentally observed in aluminum nanoparticles [119, 120]. It is interesting to note that the ΔT_m between bulk samples of Al (red brown dashed line) and Al-10Zn (purple dashed line) is also roughly observable between simulations of Al-10Zn (blue solid line) and experimental results of Al (yellow and orange solid lines) for r < 4 nm.

Despite the low temperature resolution in our tests, it is demonstrated that melting-point predictions with the grain method (blue solid line) properly converges to the bulk melting temperature (purple dashed line). These results show the potency of classical MD for studying multicomponent nanoparticles. One of the most interesting aspects of this methodology is that there is no risk of negatively impacting the cohesive energy of the lattice by using microstructural defects, since at a high enough cell volume the melting temperature will tend towards the same value as in simulations with simpler methodologies, at a much higher computational cost however.

4. Conclusion and perspectives

A comprehensive study on current classical MD approaches for melting temperature determination has been performed. The inspected procedures were 1. the void method, 2. the interface method, and 3. the grain method. The so-called void method has been extended to illustrate the effect of the vacancies' spatial distribution (within the initial crystal) on the solid-liquid phase transition. The interface method displayed the best melting point prediction for Al-FCC and for two binary compounds : Al_3Zr $D0_{23}$ and ω-Al_4Cr. Nevertheless, results from the AlLi-B32 simulations revealed the importance of the chemical environment for void sublattices. More precisely, it has been shown that the stability of this phase is increased by specifically imposing vacancies within Li-sites. This is in agreement with the free-energy modeling of this phase within thermochemical packages. Moreover, the prediction of the melting point using vacancy-based methodologies within Li sublattices led to convergence to the thermodynamic melting (critically assessed value). Lastly, the grain method provided an appropriate trend on the melting behavior for the Al-10at%Zn alloy. However, it was shown that large simulation boxes are required to properly simulate the melting with this procedure, causing a high computational cost. Based on this study, we provide the following practical recommendations for classical MD simulations:

- For pure FCC metals, the melting temperature (T_m) can be accurately predicted by the thermodynamic equation of Belonshko, which only requires a straightforward melting simulation of a crystal with no defects. Prediction of T_m using the interface method is also precise when compared to classical thermodynamics; however, its implementation demands more simulation steps and challenges compared to the Belonshko methodology.

- T_m was better estimated for congruently melting metals when using the no-defect low-temperature crystallography as the initial configuration for a melting test.

- For peritectic melting stoichiometric line compounds the interface method best evaluates T_m as the structure would otherwise not be significantly impacted by vacancies from the void method, overestimating the melting temperature.

- That the interface method, when appropriately setup and equilibrated, is suitable to model the solidus and liquids lines of binary alloys if the crystallographic reference state of pure elements provides a broad miscibility of the alloying element to form stable solid solutions (e.g. the Al-Zn system). However, it fails when describing the melting of solid solutions that naturally contain vacancies as reported in their critically assessed modeling (computational thermochemistry).

- For high-order solid solutions accepting high amounts of vacancies (e.g. the AlLi-B32), local regions with specific vacancy sublattices should be implemented as they are the initiation sites for the melting process.

- That the grain method is able to describe the melting point depression, and therefore it becomes a powerful MD approach for designing metallic nanoparticles.

5. Acknowledgements

6. CRediT authorship contribution statement

Camille Rincent: Methodology, Formal analysis, Conceptualization, Investigation, Writing - original draft. **Ricardo Castillo:** Methodology, Formal analysis, Conceptualization, Investigation, Writing - original draft. **Aïmen E. Gheribi:** Supervision, Funding acquisition, Methodology, Formal analysis, Conceptualization, Investigation, Writing - original draft. **Jean-Philippe Harvey:** Supervision, Funding acquisition, Resources, Methodology, Formal analysis, Conceptualization, Investigation, Writing - original draft.

7. Declaration of competing interest

The authors declare that they have no known competing financial interests or personal relationshops that could have appeared to influence the work reported in this paper.

8. Data Availability

Data will be made available on request.

9. Appendix: Force field formalism and development

The Second Nearest-Neighbor Modified Embedded-Atom-Method (2NN-MEAM) [121, 40, 38, 122] was used to modulate the interatomic interactions in our work. Force fields based on the 2NN-MEAM formalism are some of the most reliable models to describe metallic systems [34, 123, 96, 124, 37]. Total energy with the 2NN-MEAM formalism is defined by two contributions; an embedding function (F) and a pair potential function (ϕ_{ij}) [122]:

$$E = \sum_i \left\{ F(\bar{\rho}_i) + \frac{1}{2} \sum_{i \neq j} S_{ij} \phi_{ij}(R_{ij}) \right\} \tag{3}$$

Where $\bar{\rho}_i$ is the background electron density at the site of the i-th particle and R_{ij} is the distance between particles i and j. S_{ij} stands for the screening factor between atoms i and j. The embedded function is given by:

$$F(\bar{\rho}_i) = A E_c \frac{\bar{\rho}_i}{\bar{\rho}^0} ln(\frac{\bar{\rho}_i}{\bar{\rho}^0}) \tag{4}$$

Where A is a specific adjustable parameter of the MEAM formalism. E_c is the cohesive energy and $\bar{\rho}^0$ is the background electron density of the reference structure. The background electron density ($\bar{\rho}_i$) is related to the angular dependent partial electron densities, $\rho_i^{(k)}$, and to the weighting parameters, $t(k)$, via equations 5 and 6.

$$\bar{\rho}_i = \rho_i^{(0)} \frac{2}{1 + e^{-\Gamma_i}} \tag{5}$$

$$\Gamma_i = \sum_{k=1}^3 t^{(k)} \left(\frac{\rho_i^{(k)}}{\rho_i^{(0)}} \right)^2 \tag{6}$$

The atomic electron density is introduced as an exponentially-decaying function with respect to distance [40, 125]:

$$\rho^{a(h)}(R) = \rho_0 e^{-\beta^{(h)}(R/r_e - 1)} \tag{7}$$

Where ρ_0 is a scaling factor, $\beta^{(h)}$ are adjustable parameters, and r_e is the nearest neighbor distance of the reference structure. For more details about the partial electron density expressions related to $\rho^{a(h)}(R)$, the reader is referred to the work of Lee *et al.* [40].

The pair potential function is estimated using the following equation:

$$\phi_{ij}(R_{ij}) = \psi(R_{ij}) + \sum_{n=1} (-1)^n (Z_2 S/Z_1)^n \psi(a^n R_{ij}). \tag{8}$$

Where Z_1 and Z_2 are the number of first and second nearest-neighbor atoms, respectively. a is the ratio between the second and first nearest neighbor distances, S is a screening function on the second nearest-neighbor interactions and $\psi(R_{ij})$ is pair function obtained with the following equation :

$$\psi_{ij}(R_{ij}) = \frac{2}{Z_1} \{ E^u(R_{ij}) - F(\bar{\rho}^0(R_{ij})) \} \tag{9}$$

The total energy per atom, $E^u(R_{ij})$, is obtained from the universal equation of state [126]:

$$E^u(R_{ij}) = -E_c \left(1 + a^* + da^{*3} \right) e^{-a^*} \tag{10}$$

With $a^* = \alpha(R_{ij}/r_e - 1)$ and $\alpha = \left(\frac{9B\Omega}{E_c} \right)^{1/2}$. Where d is an adjustable parameter. E_c is the cohesive energy, r_e is the equilibrium distance, B is the bulk modulus, and Ω is the equilibrium atomic

26

volume of the reference structure.

Finally, The many-body screening function (S_{ij} in equation 3) is calculated *via* equations 11 and 12 [122].

$$S_{ij} = \prod_{k \neq i,j} S_{ikj} \tag{11}$$

$$S_{ikj} = f_c \left[\frac{C - C_{min}}{C_{max} - C_{min}} \right] \tag{12}$$

Where the triplet "ikj" represents the ij pair being screened by a third neighbor k. f_c is the smooth cutoff function [40]. C_{min} and C_{max} are the limiting values of C (equation 13), which is a geometrical parameter derived from the ellipse's equation between the ij pair, and varies according to the $i - k$ and $k - j$ distances (R_{ik} and R_{kj}, respectively).

$$C = \frac{2(X_{ik} + X_{kj}) - (X_{ik} - X_{kj})^2 - 1}{1 - (X_{ik} - X_{kj})^2} \tag{13}$$

with $X_{ik} = (R_{ik}/R_{ij})^2$ and $(X_{kj} = (R_{kj}/R_{ij})^2$.

The optimized parameters to describe the pairwise interactions of pure metals (*via* the 2NN-MEAM formalism) are presented in Table 3. They were obtained from the literature [38, 41, 40, 76, 37, 77].

Table 3: 2NN-MEAM potential parameter sets for pure elements. Units for cohesive energy E_c, equilibrium nearest-neighbor distance r_e and bulk modulus B are eV, Å, and GPa, respectively.

	Ref.	Structure	E_c	r_e	B	A	$\beta^{(0)}$	$\beta^{(1)}$	$\beta^{(2)}$	$\beta^{(3)}$	$t^{(1)}$	$t^{(2)}$	$t^{(3)}$	C_{min}	C_{max}	d
Al	[38]	FCC	3.36	2.86	79.39	1.16	3.20	2.60	6.00	2.60	3.05	0.51	7.75	0.49	2.80	0.05
Zn	[41]	HCP	1.09	2.77	70.50	0.70	3.50	3.00	0.00	2.00	3.00	6.00	-10.00	1.00	2.80	0.05
Cr	[40]	BCC	4.10	2.50	190.08	0.42	6.84	1.00	1.00	1.00	0.30	5.90	-10.40	0.78	2.80	0.05
Zr	[76]	HCP	6.36	3.20	96.77	0.68	2.45	1.00	3.00	2.00	6.30	-3.30	-10.00	1.00	1.44	0.00
Zr	[37]	BCC	6.29	3.10	89.99	0.95	3.30	1.00	1.00	1.00	5.80	-0.35	-1.30	0.25	2.80	0.00
Li	[77]	BCC	1.65	3.02	13.30	0.95	1.65	1.00	4.00	1.00	2.30	5.00	0.50	0.16	2.80	0.05

The 2NN-MEAM parameters for binary interactions for Al-Zn, Al-Zr (with the HCP-allotrope for Zr), and Al-Li are presented in Table 4. The validation of these force fields to the description of solid and liquid phases are presented in the Electronic Supplementary Information (**ESI**) of this work. For liquids, the enthalpy of mixing curves was analyzed to determine the accuracy of the 2NN-MEAM interatomic potential. For solids, the enthalpy of formation at the ground state was evaluated. These thermodynamic properties were systematically compared with available experimental data, first principle calculations, and classical thermodynamics calculations (**ESI**). The Al-Cr and Al-Zr (with the Zr-BCC reference) force fields were obtained from the literature [37]

Table 4: 2NN-MEAM potential parameter sets for binary A-B interactions (A=Al and B=Zn,Zr,Li). Units for cohesive energy E_c, equilibrium nearest-neighbor distance r_e and bulk modulus B are eV, Å, and GPa, respectively. Note that the screening parameters are displayed according to the KISSMD format, i.e. $C_{min,max}(i-k-j)$ (with the ij pair screened by k). When using the LAMMPS package, they should be adjusted as $C_{min,max}(i-j-k)$.

	Al-Zn	Al-Zr (with Zr-BCC)	Al-Li
Reference	Al$_3$Zn (L1$_2$)	Al$_3$Zr (L1$_2$)	AlLi$_3$ (L1$_2$)
E_c	2.768	4.575	2.180
r_e	2.837	2.911	2.943
B	75.0	99.0	30.0
$C_{min}(A-B-A)$	0.81	0.16	0.16
$C_{min}(B-A-B)$	0.81	0.64	0.49
$C_{min}(A-A-B)$	0.25	0.81	0.30
$C_{min}(A-B-B)$	0.25	0.81	0.30
$C_{max}(A-B-A)$	2.80	1.44	2.80
$C_{max}(B-A-B)$	2.80	2.80	2.80
$C_{max}(A-A-B)$	2.80	2.80	2.80
$C_{max}(A-B-B)$	2.80	2.80	2.80
d	0.05	0.0375	0.05
$\rho_0^A : \rho_0^B$	1:1	1:1	1:1

References

[1] Easo P George, Dierk Raabe, and Robert O Ritchie. "High-entropy alloys". In: *Nature Reviews Materials* 4.8 (2019), pp. 515–534. ISSN: 2058-8437. DOI: 10.1038/s41578-019-0121-4. URL: https://doi.org/10.1038/s41578-019-0121-4.

[2] W. Andreoni, A. Curioni, and T. Mordasini. "DFT-based molecular dynamics as a new tool for computational biology: First applications and perspective". In: *IBM Journal of Research and Development* 45.3.4 (2001), pp. 397–407. DOI: 10.1147/rd.453.0397.

[3] Patrick L.J. Conway et al. "High entropy alloys towards industrial applications: High-throughput screening and experimental investigation". In: *Materials Science and Engineering: A* 830 (2022), p. 142297. ISSN: 0921-5093. DOI: https://doi.org/10.1016/j.msea.2021.142297. URL: https://www.sciencedirect.com/science/article/pii/S0921509321015616.

[4] Jiying Wang et al. "Study of high temperature friction and wear performance of (CoCrFeMnNi)85Ti15 high-entropy alloy coating prepared by plasma cladding". In: *Surface and Coatings Technology* 384 (2020), p. 125337. ISSN: 0257-8972. DOI: https://doi.org/10.1016/j.surfcoat.2020.125337. URL: https://www.sciencedirect.com/science/article/pii/S0257897220300062.

[5] Jithin Joseph et al. "The sliding wear behaviour of CoCrFeMnNi and AlxCoCrFeNi high entropy alloys at elevated temperatures". In: *Wear* 428-429 (2019), pp. 32–44. ISSN: 0043-1648. DOI: https://doi.org/10.1016/j.wear.2019.03.002. URL: https://www.sciencedirect.com/science/article/pii/S0043164818315047.

[6] Modupeola Dada et al. "High Entropy Alloys for Aerospace Applications". In: *Aerodynamics*. Ed. by Mofid Gorji-Bandpy and Aly-Mousaad Aly. Rijeka: IntechOpen, 2019. Chap. 7. DOI: 10.5772/intechopen.84982. URL: https://doi.org/10.5772/intechopen.84982.

[7] Jitesh H. Panchal, Surya R. Kalidindi, and David L. McDowell. "Key computational modeling issues in Integrated Computational Materials Engineering". In: *Computer-Aided Design* 45.1 (2013). Computer-aided multi-scale materials and product design, pp. 4–25. ISSN: 0010-4485. DOI: https://doi.org/10.1016/j.cad.2012.06.006. URL: https://www.sciencedirect.com/science/article/pii/S0010448512001352.

[8] Wei Xiong and Gregory B Olson. "Integrated computational materials design for high-performance alloys". In: *MRS Bulletin* 40.12 (2015), pp. 1035–1044. ISSN: 1938-1425. DOI: 10.1557/mrs.2015.273. URL: https://doi.org/10.1557/mrs.2015.273.

[9] "An Introduction to Integrated Computational Materials Engineering (ICME)". In: *Integrated Computational Materials Engineering (ICME) for Metals*. John Wiley Sons, Ltd, 2012. Chap. 1, pp. 1–44. ISBN: 9781118342664. DOI: https://doi.org/10.1002/9781118342664.ch1. eprint: https://onlinelibrary.wiley.com/doi/pdf/10.1002/9781118342664.ch1. URL: https://onlinelibrary.wiley.com/doi/abs/10.1002/9781118342664.ch1.

[10] Michael Widom et al. "Hybrid Monte Carlo/Molecular Dynamics Simulation of a Refractory Metal High Entropy Alloy". In: *Metallurgical and Materials Transactions A* 45.1 (2014), pp. 196–200. ISSN: 1543-1940. DOI: 10.1007/s11661-013-2000-8. URL: https://doi.org/10.1007/s11661-013-2000-8.

[11] J.-P Harvey, A E Gheribi, and P Chartrand. "Accurate determination of the Gibbs energy of Cu-Zr melts using the thermodynamic integration method in Monte Carlo simulations ARTICLES YOU MAY BE INTERESTED IN". In: *J. Chem. Phys* 135 (2011), p. 84502. DOI: 10.1063/1.3624530. URL: https://doi.org/10.1063/1.3624530.

[12] Julien Lam, Jonathan Amodeo, and Fabio Pietrucci. "Out-of-equilibrium polymorph selection in nanoparticle freezing". In: *Journal of Physical Chemistry Letters* 11 (19 Oct. 2020), pp. 8060–8066. ISSN: 19487185. DOI: 10.1021/ACS.JPCLETT.0C02129/ASSET/IMAGES/ACS.JPCLETT.0C02129.SOCIAL.JPEG_V03. URL: https://pubs.acs.org/doi/full/10.1021/acs.jpclett.0c02129.

[13] Jean-Philippe Harvey and Paul D Asimow. "Current limitations of molecular dynamic simulations as probes of thermo-physical behavior of silicate melts". In: *American Mineralogist* 100.8-9 (2015), pp. 1866–1882.

[14] Erik C Neyts and Annemie Bogaerts. "Combining molecular dynamics with Monte Carlo simulations: implementations and applications BT - Theoretical Chemistry in Belgium: A Topical Collection from Theoretical Chemistry Accounts". In: ed. by Benoît Champagne et al. Berlin, Heidelberg: Springer Berlin Heidelberg, 2014, pp. 277–288. ISBN: 978-3-642-41315-5. DOI: 10.1007/978-3-642-41315-5_23. URL: https://doi.org/10.1007/978-3-642-41315-5_23.

[15] Xin Wang and Wei Xiong. "Uncertainty quantification and composition optimization for alloy additive manufacturing through a CALPHAD-based ICME framework". In: *npj Computational Materials* 6.1 (2020), p. 188. ISSN: 2057-3960. DOI: 10.1038/s41524-020-00454-9. URL: https://doi.org/10.1038/s41524-020-00454-9.

[16] "Discrete Dislocation Dynamics Simulations". In: *Integrated Computational Materials Engineering (ICME) for Metals*. John Wiley Sons, Ltd, 2012. Chap. 4, pp. 128–145. ISBN: 9781118342664. DOI: https://doi.org/10.1002/9781118342664.ch4. eprint: https://onlinelibrary.wiley.com/doi/pdf/10.1002/9781118342664.ch4. URL: https://onlinelibrary.wiley.com/doi/abs/10.1002/9781118342664.ch4.

[17] "Atomistic Modeling Methods". In: *Integrated Computational Materials Engineering (ICME) for Metals*. John Wiley Sons, Ltd, 2012. Chap. 5, pp. 146–163. ISBN: 9781118342664. DOI: https://doi.org/10.1002/9781118342664.ch5. eprint: https://onlinelibrary.wiley.com/doi/pdf/10.1002/9781118342664.ch5. URL: https://onlinelibrary.wiley.com/doi/abs/10.1002/9781118342664.ch5.

[18] Y.P. Wang et al. "Microstructure and compressive properties of AlCrFeCoNi high entropy alloy". In: *Materials Science and Engineering: A* 491.1 (2008), pp. 154–158. ISSN: 0921-5093. DOI: https://doi.org/10.1016/j.msea.2008.01.064. URL: https://www.sciencedirect.com/science/article/pii/S0921509308001123.

[19] Woei-Ren Wang et al. "Effects of Al addition on the microstructure and mechanical property of AlxCoCrFeNi high-entropy alloys". In: *Intermetallics* 26 (2012), pp. 44–51. ISSN: 0966-9795. DOI: https://doi.org/10.1016/j.intermet.2012.03.005. URL: https://www.sciencedirect.com/science/article/pii/S096697951200088X.

[20] David L Olmsted et al. "Atomistic simulations of dislocation mobility in Al, Ni and Al/Mg alloys". In: *Modelling and Simulation in Materials Science and Engineering* 13.3 (Mar. 2005), pp. 371–388. DOI: 10.1088/0965-0393/13/3/007. URL: https://doi.org/10.1088/0965-0393/13/3/007.

[21] Shuai Xu et al. "Molecular dynamics simulations of nano-indentation and wear of the γ-Ti-Al alloy". In: *Computational Materials Science* 110 (2015), pp. 247–253. ISSN: 0927-0256. DOI: https://doi.org/10.1016/j.commatsci.2015.08.045. URL: https://www.sciencedirect.com/science/article/pii/S0927025615005546.

[22] S. Tutunchilar et al. "Simulation of material flow in friction stir processing of a cast Al–Si alloy". In: *Materials Design* 40 (2012), pp. 415–426. ISSN: 0261-3069. DOI: https://doi.org/10.1016/j.matdes.2012.04.001. URL: https://www.sciencedirect.com/science/article/pii/S026130691200235X.

[23] Qi Hu et al. "Thermal analyses and simulations of the type A and type B Portevin–Le Chatelier effects in an Al–Mg alloy". In: *Acta Materialia* 60.4 (2012), pp. 1647–1657. ISSN: 1359-6454. DOI: https://doi.org/10.1016/j.actamat.2011.12.003. URL: https://www.sciencedirect.com/science/article/pii/S1359645411008652.

[24] D Farkas et al. "Atomistic simulations in ternary Ni - Ti - Al alloys". In: *Modelling and Simulation in Materials Science and Engineering* 4.4 (July 1996), pp. 359–369. DOI: 10.1088/0965-0393/4/4/003. URL: https://doi.org/10.1088/0965-0393/4/4/003.

[25] Rui Chen, Qingyan Xu, and Baicheng Liu. "Cellular automaton simulation of three-dimensional dendrite growth in Al–7Si–Mg ternary aluminum alloys". In: *Computational Materials Science* 105 (2015), pp. 90–100. ISSN: 0927-0256. DOI: https://doi.org/10.1016/j.commatsci.2015.04.035. URL: https://www.sciencedirect.com/science/article/pii/S0927025615002736.

[26] X. Doré, H. Combeau, and M. Rappaz. "Modelling of microsegregation in ternary alloys: Application to the solidification of Al–Mg–Si". In: *Acta Materialia* 48.15 (2000), pp. 3951–3962. ISSN: 1359-6454. DOI: https://doi.org/10.1016/S1359-6454(00)00177-4. URL: https://www.sciencedirect.com/science/article/pii/S1359645400001774.

[27] Jingwu Pi et al. "Ab initio molecular dynamics studies on effect of Zr on oxidation resistance of TiAlN coatings". In: *Applied Surface Science* 378 (2016), pp. 293–300. ISSN: 0169-4332. DOI: https://doi.org/10.1016/j.apsusc.2016.04.002. URL: https://www.sciencedirect.com/science/article/pii/S0169433216307413.

[28] Qingxin Kang et al. "Theoretical research for oxidation mechanism of α-Ti: A combination of DFT and ab initio molecular dynamics study". In: *Vacuum* 193 (2021), p. 110522. ISSN: 0042-207X. DOI: https://doi.org/10.1016/j.vacuum.2021.110522. URL: https://www.sciencedirect.com/science/article/pii/S0042207X21004711.

[29] Nick Papior et al. "Improvements on non-equilibrium and transport Green function techniques: The next-generation transiesta". In: *Computer Physics Communications* 212 (2017), pp. 8–24. ISSN: 0010-4655. DOI: https://doi.org/10.1016/j.cpc.2016.09.022. URL: https://www.sciencedirect.com/science/article/pii/S001046551630306X.

[30] Yanpeng Shang et al. "The computational study of microchannel thickness effects on H2O/CuO nanofluid flow with molecular dynamics simulations". In: *Journal of Molecular Liquids* 345 (2022), p. 118240. ISSN: 0167-7322. DOI: https://doi.org/10.1016/j.molliq.2021.118240. URL: https://www.sciencedirect.com/science/article/pii/S0167732221029652.

[31] Hui Yao et al. "Discussion on molecular dynamics (MD) simulations of the asphalt materials". In: *Advances in Colloid and Interface Science* 299 (2022), p. 102565. ISSN: 0001-8686. DOI: https://doi.org/10.1016/j.cis.2021.102565. URL: https://www.sciencedirect.com/science/article/pii/S0001868621002062.

[32] Q.X. Pei, C. Lu, and H.P. Lee. "Large scale molecular dynamics study of nanometric machining of copper". In: *Computational Materials Science* 41.2 (2007), pp. 177–185. ISSN: 0927-0256. DOI: https://doi.org/10.1016/j.commatsci.2007.04.008. URL: https://www.sciencedirect.com/science/article/pii/S0927025607000869.

[33] Sedigheh Bigdeli et al. "An insight into using DFT data for Calphad modeling of solid phases in the third generation of Calphad databases, a case study for Al". In: *Calphad* 65 (2019), pp. 79–85. ISSN: 0364-5916. DOI: https://doi.org/10.1016/j.calphad.2019.02.008. URL: https://www.sciencedirect.com/science/article/pii/S0364591618301718.

[34] Young-Kwang Kim et al. "Development and application of Ni-Ti and Ni-Al-Ti 2NN-MEAM interatomic potentials for Ni-base superalloys". In: *Computational Materials Science* 139 (2017), pp. 225–233. ISSN: 0927-0256. DOI: https://doi.org/10.1016/j.commatsci.2017.08.002. URL: https://www.sciencedirect.com/science/article/pii/S0927025617304081.

[35] Yunqing Tang and D.Y. Li. "Nano-tribological behavior of high-entropy alloys CrMnFeCoNi and CrFeCoNi under different conditions: A molecular dynamics study". In: *Wear* 476 (2021). 23rd International Conference on Wear of Materials, p. 203583. DOI: https://doi.org/10.1016/j.wear.2020.203583.

[36] Zhenwei Wu et al. "Molecular Dynamics Investigation of the Influence of Voids on the Impact Mechanical Behavior of NiTi Shape-Memory Alloy". In: *Materials* 14.14 (2021). DOI: 10.3390/ma14144020.

[37] Juan-Ricardo Castillo-Sánchez et al. "On the transferability of classical pairwise additive atomistic force field to the description of unary and multi-component systems: applications to the solidification of Al-based alloys". In: *Phys. Chem. Chem. Phys.* 24 (37 2022), pp. 22605–22623. DOI: 10.1039/D2CP02746A. URL: http://dx.doi.org/10.1039/D2CP02746A.

[38] Byeong-Joo Lee, Jae-Hyeok Shim, and M. I. Baskes. "Semiempirical atomic potentials for the fcc metals Cu, Ag, Au, Ni, Pd, Pt, Al, and Pb based on first and second nearest-neighbor modified embedded atom method". In: *Phys. Rev. B* 68 (14 Oct. 2003), p. 144112. DOI: 10.1103/PhysRevB.68.144112. URL: https://link.aps.org/doi/10.1103/PhysRevB.68.144112.

[39] Hyo-Sun Jang, Donghyuk Seol, and Byeong-Joo Lee. "Modified embedded-atom method interatomic potentials for Mg–Al–Ca and Mg–Al–Zn ternary systems". In: *Journal of Magnesium and Alloys* 9.1 (2021), pp. 317–335. DOI: https://doi.org/10.1016/j.jma.2020.09.006. URL: https://www.sciencedirect.com/science/article/pii/S2213956720301559.

[40] Byeong-Joo Lee et al. "Second nearest-neighbor modified embedded atom method potentials for bcc transition metals". In: *Phys. Rev. B* 64 (18 Oct. 2001), p. 184102. DOI: 10.1103/PhysRevB.64.184102. URL: https://link.aps.org/doi/10.1103/PhysRevB.64.184102.

[41] Hyo-Sun Jang, Kyeong-Min Kim, and Byeong-Joo Lee. "Modified embedded-atom method interatomic potentials for pure Zn and Mg-Zn binary system". In: *Calphad* 60 (2018), pp. 200–207. ISSN: 0364-5916. DOI: https://doi.org/10.1016/j.calphad.2018.01.003. URL: https://www.sciencedirect.com/science/article/pii/S0364591617302055.

[42] M. I. Baskes. "Modified embedded-atom potentials for cubic materials and impurities". In: *Phys. Rev. B* 46 (5 Aug. 1992), pp. 2727–2742. DOI: 10.1103/PhysRevB.46.2727. URL: https://link.aps.org/doi/10.1103/PhysRevB.46.2727.

[43] Kazuhiro Yamada et al. "Evaluation of thermal properties of uranium dioxide by molecular dynamics". In: *Journal of Alloys and Compounds* 307.1 (2000), pp. 10–16. ISSN: 0925-8388. DOI: https://doi.org/10.1016/S0925-8388(00)00806-9. URL: https://www.sciencedirect.com/science/article/pii/S0925838800008069.

[44] Giorgio Mazzone et al. "Molecular-dynamics calculations of thermodynamic properties of metastable alloys". In: *Phys. Rev. B* 55 (2 Jan. 1997), pp. 837–842. DOI: 10.1103/PhysRevB.55.837. URL: https://link.aps.org/doi/10.1103/PhysRevB.55.837.

[45] Azar Shamloo, Denis Rodrigue, and Armand Soldera. "Melting of alkane nanocrystals: towards a representation of polyethylene". In: *Molecular Simulation* 47.10-11 (2021), pp. 900–904. DOI: 10.1080/08927022.2020.1797020. eprint: https://doi.org/10.1080/08927022.2020.1797020. URL: https://doi.org/10.1080/08927022.2020.1797020.

[46] S. Alireza Etesami and Ebrahim Asadi. "Molecular dynamics for near melting temperatures simulations of metals using modified embedded-atom method". In: *Journal of Physics and Chemistry of Solids* 112 (2018), pp. 61–72. ISSN: 0022-3697. DOI: https://doi.org/10.1016/j.jpcs.2017.09.001. URL: https://www.sciencedirect.com/science/article/pii/S0022369717312039.

[47] Tomasz Wejrzanowski et al. "Effect of grain size on the melting point of confined thin aluminum films". In: 116 (2014). DOI: 10.1063/1.4899240JournalName:JournalofAppliedPhysics;JournalVolume:116;JournalIssue:16;OtherInformation:(c)2014AIPPublishingLLC;Countryofinput:InternationalAtomicEnergyAgency(IAEA). URL: https://www.osti.gov/biblio/22308180.

[48] Zahra Noori, Masoud Panjepour, and Mehdi Ahmadian. "Study of the effect of grain size on melting temperature of Al nanocrystals by molecular dynamics simulation". In: *Journal of Materials Research* 30.10 (2015), pp. 1648–1660. DOI: 10.1557/jmr.2015.109.

[49] Y. Tang and L. Zhang. "Effect of Thermal Vacancy on Thermodynamic Behaviors in BCC W Close to Melting Point: A Thermodynamic Study". In: *Materials (Basel)* 11.9 (2018). ISSN: 1996-1944 (Print) 1996-1944. DOI: 10.3390/ma11091648.

[50] GÖRAN GRIMVALL. "CHAPTER 2 - CRYSTAL DEFECTS". In: *Thermophysical Properties of Materials*. Ed. by GÖRAN GRIMVALL. Amsterdam: Elsevier Science B.V., 1999, pp. 18–26. ISBN: 978-0-444-82794-4. DOI: https://doi.org/10.1016/B978-044482794-4/50003-6. URL: https://www.sciencedirect.com/science/article/pii/B9780444827944500036.

[51] Laia Delgado-Callico et al. "A universal signature in the melting of metallic nanoparticles". In: *Nanoscale* 13 (2 Jan. 2021), pp. 1172–1180. ISSN: 2040-3372. DOI: 10.1039/D0NR06850K. URL: https://pubs.rsc.org/en/content/articlehtml/2021/nr/d0nr06850k%20https://pubs.rsc.org/en/content/articlelanding/2021/nr/d0nr06850k.

[52] Paras M. Agrawal, Betsy M. Rice, and Donald L. Thompson. "Molecular dynamics study of the effects of voids and pressure in defect-nucleated melting simulations". In: *The Journal of Chemical Physics* 118.21 (2003), pp. 9680–9688. DOI: 10.1063/1.1570815. eprint: https://doi.org/10.1063/1.1570815. URL: https://doi.org/10.1063/1.1570815.

[53] Yong Zhang and Edward J. Maginn. "A comparison of methods for melting point calculation using molecular dynamics simulations". In: *The Journal of Chemical Physics* 136.14 (2012), p. 144116. DOI: 10.1063/1.3702587. eprint: https://doi.org/10.1063/1.3702587. URL: https://doi.org/10.1063/1.3702587.

[54] YangChun Zou, ShiKai Xiang, and ChengDa Dai. "Investigation on the efficiency and accuracy of methods for calculating melting temperature by molecular dynamics simulation". In: *Computational Materials Science* 171 (2020), p. 109156. ISSN: 0927-0256. DOI: https://doi.org/10.1016/j.commatsci.2019.109156. URL: https://www.sciencedirect.com/science/article/pii/S0927025619304550.

[55] Xuehao Yu et al. "On the affected strength of Al grain boundaries by Zn segregation: A first-principles interpretation". In: *Computational Materials Science* 212 (2022), p. 111604. ISSN: 0927-0256. DOI: https://doi.org/10.1016/j.commatsci.2022.111604. URL: https://www.sciencedirect.com/science/article/pii/S0927025622003482.

[56] Qicheng Chen et al. "Influence of Vacancy Defects of the Calcium Oxide Surface on the Nonequilibrium Phase Transition of Alkali Metal Salts". In: *Langmuir* 38.2 (2022). PMID: 34985909, pp. 818–827. DOI: 10.1021/acs.langmuir.1c02851. eprint: https://doi.org/10.1021/acs.langmuir.1c02851. URL: https://doi.org/10.1021/acs.langmuir.1c02851.

[57] Jing Peng et al. "Vacancy dependent mechanical behaviors of high-entropy alloy". In: *International Journal of Mechanical Sciences* 218 (2022), p. 107065. ISSN: 0020-7403. DOI: https://doi.org/10.1016/j.ijmecsci.2022.107065. URL: https://www.sciencedirect.com/science/article/pii/S0020740322000030.

[58] Mashhour A. Alazwari et al. "Vacancy defect influence on nanofluid flow and absorbed thermal energy in a nanochannel affected by Universal Force Field via composed approach of embedded atom model/molecular dynamics method". In: *Journal of Molecular Liquids* 333 (2021), p. 115927. ISSN: 0167-7322. DOI: https://doi.org/10.1016/j.molliq.2021.115927. URL: https://www.sciencedirect.com/science/article/pii/S0167732221006541.

[59] James R. Morris and Xueyu Song. "The melting lines of model systems calculated from coexistence simulations". In: *The Journal of Chemical Physics* 116.21 (2002), pp. 9352–9358. DOI: 10.1063/1.1474581. eprint: https://doi.org/10.1063/1.1474581. URL: https://doi.org/10.1063/1.1474581.

[60] Stephen W. Watt et al. "A molecular dynamics simulation of the melting points and glass transition temperatures of myo- and neo-inositol". In: *The Journal of Chemical Physics* 121.19 (2004), pp. 9565–9573. DOI: 10.1063/1.1806792. eprint: https://doi.org/10.1063/1.1806792. URL: https://doi.org/10.1063/1.1806792.

[61] Yang Chun Zou, Shi Kai Xiang, and Cheng Da Dai. "Investigation on the efficiency and accuracy of methods for calculating melting temperature by molecular dynamics simulation". In: *Computational Materials Science* 171 (Jan. 2020), p. 109156. ISSN: 0927-0256. DOI: 10.1016/J.COMMATSCI.2019.109156.

[62] Byeong Joo Lee, Jae Hyeok Shim, and I. Baskes. "Semiempirical atomic potentials for the fcc metals Cu, Ag, Au, Ni, Pd, Pt, Al, and Pb based on first and second nearest-neighbor modified embedded atom method". In: *Physical Review B* 68 (14 Oct. 2003), p. 144112. ISSN: 1550235X. DOI: 10.1103/PhysRevB.68.144112. URL: https://journals.aps.org/prb/abstract/10.1103/PhysRevB.68.144112.

[63] Saman Alavi and Donald L. Thompson. "Molecular dynamics studies of melting and some liquid-state properties of 1-ethyl-3-methylimidazolium hexafluorophosphate [emim][PF6]". In: *The Journal of Chemical Physics* 122 (15 Apr. 2005), p. 154704. ISSN: 0021-9606. DOI: 10.1063/1.1880932. URL: https://aip.scitation.org/doi/abs/10.1063/1.1880932.

[64] Paras M. Agrawal et al. "Molecular dynamics simulations of the melting of 1,3,3-trinitroazetidine". In: *Journal of Physical Chemistry B* 110 (11 Mar. 2006), pp. 5721–5726. ISSN: 15206106. DOI: 10.1021/JP056690G/ASSET/IMAGES/LARGE/JP056690GF00004.JPEG. URL: https://pubs.acs.org/doi/full/10.1021/jp056690g.

[65] Amitava Moitra et al. "Melting tungsten nanoparticles: a molecular dynamics study". In: *Journal of Physics D: Applied Physics* 41 (18 Aug. 2008), p. 185406. ISSN: 0022-3727. DOI: 10.1088/0022-3727/41/18/185406. URL: https://iopscience.iop.org/article/10.1088/0022-3727/41/18/185406%20https://iopscience.iop.org/article/10.1088/0022-3727/41/18/185406/meta.

[66] Zhiwei Cui et al. "Developing a second nearest-neighbor modified embedded atom method interatomic potential for lithium". In: *Modelling and Simulation in Materials Science and Engineering* 20 (1 Dec. 2011), p. 015014. ISSN: 0965-0393. DOI: 10.1088/0965-0393/20/1/015014. URL: https://iopscience.iop.org/article/10.1088/0965-0393/20/1/015014%20https://iopscience.iop.org/article/10.1088/0965-0393/20/1/015014/meta.

[67] A. V. Fedorov and A. V. Shulgin. "Molecular dynamics modeling melting of of aluminum nanoparticles of the embedded atom method". In: *Combustion, Explosion and Shock Waves* 51 (3 May 2015), pp. 333–337. ISSN: 15738345. DOI: 10.1134/S0010508215030089/METRICS. URL: https://link.springer.com/article/10.1134/S0010508215030089.

[68] Ebrahim Asadi et al. "Two-phase solid–liquid coexistence of Ni, Cu, and Al by molecular dynamics simulations using the modified embedded-atom method". In: *Acta Materialia* 86 (Mar. 2015), pp. 169–181. ISSN: 1359-6454. DOI: 10.1016/J.ACTAMAT.2014.12.010.

[69] Weimiao Lv et al. "Development of modified embedded-atom model and molecular dynamics simulation of cesium". In: *Computational Materials Science* 194 (June 2021), p. 110451. ISSN: 0927-0256. DOI: 10.1016/J.COMMATSCI.2021.110451.

[70] Avik Mahata, Tanmoy Mukhopadhyay, and Mohsen Asle Zaeem. "Modified embedded-atom method interatomic potentials for Al-Cu, Al-Fe and Al-Ni binary alloys: From room temperature to melting point". In: *Computational Materials Science* 201 (Jan. 2022), p. 110902. ISSN: 0927-0256. DOI: 10.1016/J.COMMATSCI.2021.110902.

[71] Changzeng Fan and Cong Liu. "Crystal structure of ω-Al¡sub¿4¡/sub¿Cr". In: *IUCrData* 3.2 (2018). ISSN: 2414-3146. DOI: 10.1107/s241431461800216x. URL: http://10.0.4.83/s241431461800216x%20https://dx.doi.org/10.1107/s241431461800216x.

[72] Sheng-Nian Luo, Alejandro Strachan, and Damian C. Swift. "Nonequilibrium melting and crystallization of a model Lennard-Jones system". In: *The Journal of Chemical Physics* 120.24 (2004), pp. 11640–11649. DOI: 10.1063/1.1755655. eprint: https://doi.org/10.1063/1.1755655. URL: https://doi.org/10.1063/1.1755655.

[73] Jess B. Sturgeon and Brian B. Laird. "Adjusting the melting point of a model system via Gibbs-Duhem integration: Application to a model of aluminum". In: *Phys. Rev. B* 62 (22 Dec. 2000), pp. 14720–14727. DOI: 10.1103/PhysRevB.62.14720. URL: https://link.aps.org/doi/10.1103/PhysRevB.62.14720.

[74] Jean-Philippe Harvey, Aïmen E Gheribi, and Patrice Chartrand. "On the determination of the glass forming ability of Al x Zr 1x alloys using molecular dynamics, Monte Carlo simulations, and classical thermodynamics". In: *J. Appl. Phys* 112 (2012), p. 73508. DOI: 10.1063/1.4756037. URL: https://doi.org/10.1063/1.4756037.

[75] Jean Philippe Harvey, Aïmen E. Gheribi, and Patrice Chartrand. "On the determination of the glass forming ability of AlxZr1x alloys using molecular dynamics, Monte Carlo simulations, and classical thermodynamics". In: *Journal of Applied Physics* 112 (7 Oct. 2012), p. 073508. ISSN: 0021-8979. DOI: 10.1063/1.4756037. URL: https://aip.scitation.org/doi/abs/10.1063/1.4756037.

[76] Young-Min Kim, Byeong-Joo Lee, and MI Baskes. "Modified embedded-atom method interatomic potentials for Ti and Zr". In: *Physical Review B* 74.1 (2006), p. 014101.

[77] Young-Min Kim, In-Ho Jung, and Byeong-Joo Lee. "Atomistic modeling of pure Li and Mg–Li system". In: *Modelling and Simulation in Materials Science and Engineering* 20 (3 Apr. 2012), p. 035005. ISSN: 0965-0393. DOI: 10.1088/0965-0393/20/3/035005. URL: https://iopscience.iop.org/article/10.1088/0965-0393/20/3/035005.

[78] A. P. Thompson et al. "LAMMPS - a flexible simulation tool for particle-based materials modeling at the atomic, meso, and continuum scales". In: *Comp. Phys. Comm.* 271 (2022), p. 108171. DOI: 10.1016/j.cpc.2021.108171.

[79] Anubhav Jain et al. "The Materials Project: A materials genome approach to accelerating materials innovation". In: *APL Materials* 1.1 (2013), p. 011002. ISSN: 2166532X. DOI: 10.1063/1.4812323. URL: http://link.aip.org/link/AMPADS/v1/i1/p011002/s1%5C&Agg=doi.

[80] Shuichi Nosé. "A unified formulation of the constant temperature molecular dynamics methods". In: *The Journal of Chemical Physics* 81.1 (1984), pp. 511–519. DOI: 10.1063/1.447334. eprint: https://doi.org/10.1063/1.447334. URL: https://doi.org/10.1063/1.447334.

[81] William G. Hoover. "Canonical dynamics: Equilibrium phase-space distributions". In: *Phys. Rev. A* 31 (3 Mar. 1985), pp. 1695–1697. DOI: 10.1103/PhysRevA.31.1695. URL: https://link.aps.org/doi/10.1103/PhysRevA.31.1695.

[82] Qiang Shu et al. "Size-dependent melting behavior of iron nanoparticles by replica exchange molecular dynamics". In: (). DOI: 10.1039/c2nr30853c. URL: www.rsc.org/nanoscale.

[83] Kaiwang Zhang, G Malcolm Stocks, and Jianxin Zhong. "Melting and premelting of carbon nanotubes". In: *Nanotechnology* 18.28 (June 2007), p. 285703. DOI: 10.1088/0957-4484/18/28/285703. URL: https://doi.org/10.1088/0957-4484/18/28/285703.

[84] Peter Mahler Larsen, Søren Schmidt, and Jakob Schiøtz. "Robust structural identification via polyhedral template matching". In: *Modelling and Simulation in Materials Science and Engineering* 24.5 (2016), p. 055007.

[85] Alexander Stukowski. "Visualization and analysis of atomistic simulation data with OVITO–the Open Visualization Tool". In: *Modelling and simulation in materials science and engineering* 18.1 (2009), p. 015012.

[86] Anatoly Belonoshko et al. "Melting and critical superheating". In: *Phys. Rev. B* 73 (Jan. 2006). DOI: 10.1103/PhysRevB.73.012201.

[87] K. Rossi et al. "Thermodynamics of CuPt nanoalloys". In: *Scientific Reports 2018 8:1* 8 (1 June 2018), pp. 1–9. ISSN: 2045-2322. DOI: 10.1038/s41598-018-27308-1. URL: https://www.nature.com/articles/s41598-018-27308-1.

[88] Søren Smidstrup et al. "QuantumATK: An integrated platform of electronic and atomic-scale modelling tools". In: *J. Phys: Condens. Matter* 32 (2020), p. 015901.

[89] F. Czerwinski. "Thermal Stability of Aluminum Alloys". In: *Materials (Basel)* 13.15 (2020). ISSN: 1996-1944 (Print) 1996-1944. DOI: 10.3390/ma13153441.

[90] S W Holman, R R Lawrence, and L Barr. *Melting Points of Aluminum, Silver, Gold, Copper, and Platinum.* 1895, pp. 218–233.

[91] Tomasz Maciag. "Enthalpy of formation of intermetallic phases from Al–Zr system determined by calorimetric solution method". In: *Journal of Thermal Analysis and Calorimetry* 134 (1 Oct. 2018), pp. 423–431. ISSN: 15882926. DOI: 10.1007/s10973-017-6917-9.

[92] A.V. Khvan et al. "New insights into solidification and phase equilibria in the Al-Al3Zr system: Theoretical and experimental investigations". In: *Journal of Alloys and Compounds* 743 (2018), pp. 626–638. ISSN: 0925-8388. DOI: https://doi.org/10.1016/j.jallcom.2018.02.023. URL: https://www.sciencedirect.com/science/article/pii/S0925838818304535.

[93] Tianxing Yang et al. "First-principle calculations on the Al/L12-Al3Zr heterogeneous nucleation interface". In: *Calphad* 69 (2020), p. 101768. ISSN: 0364-5916. DOI: https://doi.org/10.1016/j.calphad.2020.101768. URL: https://www.sciencedirect.com/science/article/pii/S036459162030033X.

[94] Emmanuel Clouet et al. "Precipitation kinetics of Al3Zr and Al3Sc in aluminum alloys modeled with cluster dynamics". In: *Acta Materialia* 53.8 (2005), pp. 2313–2325. ISSN: 1359-6454. DOI: https://doi.org/10.1016/j.actamat.2005.01.038. URL: https://www.sciencedirect.com/science/article/pii/S1359645405000674.

[95] Tianxing Yang et al. "Electronic and structural properties of low-index L12–Al3Zr surfaces by first-principle calculations". In: *Calphad* 66 (2019), p. 101645. ISSN: 0364-5916. DOI: https://doi.org/10.1016/j.calphad.2019.101645. URL: https://www.sciencedirect.com/science/article/pii/S0364591619300549.

[96] J-P Harvey, AE Gheribi, and P Chartrand. "Thermodynamic integration based on classical atomistic simulations to determine the Gibbs energy of condensed phases: Calculation of the aluminum-zirconium system". In: *Physical Review B* 86.22 (2012), p. 224202.

[97] Lipeng Ding et al. "On the formation of anti-phase boundaries and interphase boundaries in Al3Zr precipitates of Al-Cu-Zr alloy studied at atomic scale". In: *Journal of Alloys and Compounds* 887 (2021), p. 161442. ISSN: 0925-8388. DOI: https://doi.org/10.1016/j.jallcom.2021.161442. URL: https://www.sciencedirect.com/science/article/pii/S0925838821028516.

[98] Emmanuel Clouet, J. M. Sanchez, and C. Sigli. "First-principles study of the solubility of Zr in Al". In: *Phys. Rev. B* 65 (9 Feb. 2002), p. 094105. DOI: 10.1103/PhysRevB.65.094105. URL: https://link.aps.org/doi/10.1103/PhysRevB.65.094105.

[99] Kamal Mahdouk and Jean-Claude Gachon. "Thermodynamic Investigation of the Aluminum-Chromium System". In: *Journal of Phase Equilibria* 21 (2 Jan. 2000), pp. 157–166.

[100] Changzeng Fan, Xu Geng, and Bin Wen. *Pressure Induced Disorder-Order Phase Transitions in the Al4Cr Phases.* 2022. DOI: 10.3390/cryst12071008.

[101] B.B. Cao. "On the structure of the hexagonal μ-Al4Cr and its relation to the monoclinic η-Al11Cr2". In: *Journal of Alloys and Compounds* 698 (2017), pp. 605–610. ISSN: 0925-8388. DOI: https://doi.org/10.1016/j.jallcom.2016.12.270. URL: https://www.sciencedirect.com/science/article/pii/S0925838816342001.

[102] T.B. Massalski et al. *Binary Alloy Phase Diagrams, 2nd Edition - ASM International.* 1990. URL: https://www.asminternational.org/online-catalog/alloy-phase-diagrams/-/journal_content/56/10192/57718G/PUBLICATION.

[103] Aftab Alam and Duane D Johnson. "Structural properties and relative stability of (meta) stable ordered, partially ordered, and disordered Al-Li alloy phases". In: *Physical Review B* 85.14 (2012), p. 144202.

[104] GP Das, A Arya, and S Banerjee. "Ground state structural stability of ordered fcc-and bcc-based Li-Al compounds under first and second nearest-neighbour pair approximation". In: *Intermetallics* 4.8 (1996), pp. 625–634.

[105] Jaakko Akola and Matti Manninen. "Aluminum-lithium clusters: First-principles simulation of geometries and electronic properties". In: *Physical Review B* 65.24 (2002), p. 245424.

[106] A J McAlister. "The AlLi (AluminumLithium) system". In: *Bulletin of Alloy Phase Diagrams* 3.2 (1982), pp. 177–183. ISSN: 0197-0216. DOI: 10.1007/BF02892377. URL: https://doi.org/10.1007/BF02892377.

[107] HL Lukas. "COST 507 Thermochemical database for light metal alloys". In: *EUR 18499 EN 2* (1998), pp. 227–233.

[108] Paul A Rometsch, Yong Zhang, and Steven Knight. "Heat treatment of 7xxx series aluminium alloys—Some recent developments". In: *Transactions of Nonferrous Metals Society of China* 24.7 (2014), pp. 2003–2017.

[109] Johannes A Österreicher et al. "Stabilization of 7xxx aluminium alloys". In: *Journal of alloys and compounds* 740 (2018), pp. 167–173.

[110] "Chapter A.3 - The Metallurgy of Aluminium". In: *Corrosion of Aluminium*. Ed. by Christian Vargel. Amsterdam: Elsevier, 2004, pp. 23–57. ISBN: 978-0-08-044495-6. DOI: https://doi.org/10.1016/B978-008044495-6/50008-2.

[111] MatWeb. *Aluminum 7034-T6.* 2001. URL: https://www.matweb.com/search/datasheet.aspx?matguid=844471e12b9e4d389b5983f26876b835&ckck=1.

[112] MatWeb. *7093 Aluminum Composition Spec.* 2001. URL: https://www.matweb.com/search/datasheet.aspx?matguid=104899d400b84416b672899b9d820b8e.

[113] Alan Dinsdale et al. "Use of third generation data for the elements to model the thermodynamics of binary alloy systems: Part 1 – The critical assessment of data for the Al-Zn system". In: *Calphad* 68 (Mar. 2020), p. 101723. ISSN: 0364-5916. DOI: 10.1016/J.CALPHAD.2019.101723.

[114] Matias Haapalehto et al. "An atomistic simulation study of rapid solidification kinetics and crystal defects in dilute Al–Cu alloys". In: *Computational Materials Science* 209 (2022), p. 111356. ISSN: 0927-0256. DOI: https://doi.org/10.1016/j.commatsci.2022.111356. URL: https://www.sciencedirect.com/science/article/pii/S0927025622001392.

[115] Kensho Ueno and Yasushi Shibuta. "Semi-grand canonical Monte Carlo simulation for derivation of thermodynamic properties of binary alloy". In: *IOP Conference Series: Materials Science and Engineering* 529 (1 June 2019). ISSN: 1757899X. DOI: 10.1088/1757-899X/529/1/012037.

[116] C. O.T. Galvin, R. W. Grimes, and P. A. Burr. "A molecular dynamics method to identify the liquidus and solidus in a binary phase diagram". In: *Computational Materials Science* 186 (Jan. 2021). ISSN: 09270256. DOI: 10.1016/J.COMMATSCI.2020.110016.

[117] M.E. Glicksman. *Principles of Solidification: An Introduction to Modern Casting and Crystal Growth Concepts.* SpringerLink : Bücher. Springer New York, 2010. ISBN: 9781441973443. URL: https://books.google.ca/books?id=rXMuZY08KfkC.

[118] B Straumal et al. "Thermal evolution and grain boundary phase transformations in severely deformed nanograined Al–Zn alloys". In: *Acta Materialia* 56.20 (2008), pp. 6123–6131. ISSN: 1359-6454. DOI: https://doi.org/10.1016/j.actamat.2008.08.021. URL: https://www.sciencedirect.com/science/article/pii/S1359645408005867.

[119] Mataz Alcoutlabi and Gregory B McKenna. "Effects of confinement on material behaviour at the nanometre size scale". In: *Journal of Physics: Condensed Matter* 17.15 (2005), R461.

[120] S L Lai, J R A Carlsson, and L H Allen. "Melting point depression of Al clusters generated during the early stages of film growth: Nanocalorimetry measurements". In: *Applied Physics Letters* 72.9 (Mar. 1998), pp. 1098–1100. ISSN: 0003-6951. DOI: 10.1063/1.120946. URL: https://doi.org/10.1063/1.120946.

[121] Byeong-Joo Lee and MI Baskes. "Second nearest-neighbor modified embedded-atom-method potential". In: *Physical Review B* 62.13 (2000), p. 8564.

[122] Byeong-Joo Lee et al. "The modified embedded-atom method interatomic potentials and recent progress in atomistic simulations". In: *Calphad* 34.4 (2010), pp. 510–522. ISSN: 0364-5916. DOI: https://doi.org/10.1016/j.calphad.2010.10.007. URL: https://www.sciencedirect.com/science/article/pii/S0364591610000817.

[123] Prashanth Srinivasan, Lucia Nicola, and Angelo Simone. "Modeling pseudo-elasticity in NiTi: Why the MEAM potential outperforms the EAM-FS potential". In: *Computational Materials Science* 134 (2017), pp. 145–152.

[124] J-P Harvey, AE Gheribi, and P Chartrand. "Accurate determination of the Gibbs energy of Cu–Zr melts using the thermodynamic integration method in Monte Carlo simulations". In: *The Journal of chemical physics* 135.8 (2011), p. 084502.

[125] J Matthew D Lane, Aidan P Thompson, and Tracy J Vogler. "Enhanced densification under shock compression in porous silicon". In: *Physical Review B* 90.13 (2014), p. 134311.

[126] James H. Rose et al. "Universal features of the equation of state of metals". In: *Phys. Rev. B* 29 (6 Mar. 1984), pp. 2963–2969. DOI: 10.1103/PhysRevB.29.2963. URL: https://link.aps.org/doi/10.1103/PhysRevB.29.2963.